nature communications

Article

https://doi.org/10.1038/s41467-024-55053-9

Myosin VI drives arrestin-independent internalization and signaling of GPCRs

Received: 30 May 2024

Accepted: 26 November 2024

Published online: 06 December 2024

Check for updates

Nishaben M. Patel[1], Léa Ripoll[2], Chloe J. Peach[3,4], Ning Ma[5,6], Emily E. Blythe[2], Nagarajan Vaidehi[5,6], Nigel W. Bunnett[3], Mark von Zastrow[2] & Sivaraj Sivaramakrishnan[1]

G protein-coupled receptor (GPCR) endocytosis is canonically associated with β-arrestins. Here, we delineate a β-arrestin-independent endocytic pathway driven by the cytoskeletal motor, myosin VI. Myosin VI engages GIPC, an adaptor protein that binds a PDZ sequence motif present at the C-terminus of several GPCRs. Using the D2 dopamine receptor (D2R) as a prototype, we find that myosin VI regulates receptor endocytosis, spatiotemporal localization, and signaling. We find that access to the D2R C-tail for myosin VI-driven internalization is controlled by an interaction between the C-tail and the third intracellular loop of the receptor. Agonist efficacy, co-factors, and GIPC expression modulate this interaction to tune agonist trafficking. Myosin VI is differentially regulated by distinct GPCR C-tails, suggesting a mechanism to shape spatiotemporal signaling profiles in different ligand and physiological contexts. Our biophysical and structural insights may advance orthogonal therapeutic strategies for targeting GPCRs through cytoskeletal motor proteins.

An emerging paradigm links receptor membrane trafficking to the precise spatiotemporal regulation of GPCR signaling[1,2]. GPCR trafficking mechanisms have focused on receptor phosphorylation by GRKs and subsequent β-arrestin recruitment, leading to internalization and distinct endomembrane signaling profiles[3]. In contrast, twenty-six distinct PDZ adaptor proteins have been shown to selectively regulate GPCR function by modulating receptor spatial localization[4]. The molecular basis of PDZ adaptor regulation of GPCRs remains elusive and forms the focus of this study[5].

PDZ adaptor proteins contain one or more PDZ protein domains that bind a PDZ binding motif (PBM)[4–6]. GPCR PBMs are typically located at the receptor C-terminus[5]. PBMs are predominantly classified into three types (I-III), with overlapping preferences for PDZ domains (type I – S/T-X-Ψ; type II - Ψ-X-Ψ; type III – X-X-C, where Ψ is a hydrophobic residue that is typically V/I/L but may include other amino acids)[5–7]. 39 distinct human GPCRs have the prototypical class I PDZ motif, with many more containing type II/III and atypical sequence motifs that are often internal to the receptor[5]. The sequence diversity of PBMs, combined with the modular organization of PDZ motifs in adaptor proteins, has the potential to differentially modulate the receptor signaling landscape[6,8]. However, this diversity of PDZ adaptor proteins, combined with their individual contextual effects on receptors has limited generalizable molecular insights akin to β-arrestin trafficking. Here, we use the D2 dopamine receptor (D2R) interaction with the PDZ adaptor GIPC to delineate a β-arrestin independent cytoskeletal pathway that regulates GPCR trafficking and signaling.

D2R is a $G\alpha_{i/o}$ coupled GPCR in the central nervous system (CNS) that is a prominent therapeutic target in Parkinson's disease, schizophrenia and major depressive disorders[9–11]. D2 and D3 receptors have

[1]Department of Genetics, Cell Biology and Development, University of Minnesota, Minneapolis, MN, USA. [2]Department of Psychiatry and Behavioral Sciences, University of California, San Francisco, San Francisco, CA, USA. [3]Department of Molecular Pathobiology, New York University, New York, NY, USA. [4]School of Life Sciences, Centre of Membrane Proteins and Receptors (COMPARE), University of Nottingham, Nottingham, UK. [5]Irell and Manella Graduate School of Biological Sciences, Beckman Research Institute of the City of Hope, Duarte, CA, USA. [6]Department of Computational and Quantitative Medicine, Beckman Research Institute of the City of Hope, Duarte, CA, USA. e-mail: sivaraj@umn.edu

been shown to interact with the PDZ adaptor GIPC (GAIP interacting protein C terminus) through a type III PBM at its C-terminus[12]. GIPC binding influences receptor trafficking and signaling[13]. However, the molecular basis for GIPC effects on D2R trafficking remain unresolved. Further, GIPC has been shown to interact with a number of GPCRs, including LPA1R, LHR, and β1AR[14–16]. In parallel, GIPC is a known adaptor of the cytoskeleton motor myosin VI[17,18]. Myosin VI is an actin-based molecular motor[19] that has been repeatedly implicated in the timely trafficking and recycling of endosomal compartments through interactions with numerous adaptor proteins[20–22]. The myosin interacting region (MIR) of GIPC enhances myosin VI motility by releasing an autoinhibitory interaction within the motor[23]. Additionally, the GIPC-myosin VI interaction has been shown to regulate trafficking of cell surface receptors including megalin[24] and receptor tyrosine kinases such as TrkA[25]. Nonetheless, while a potential role for this cytoskeletal motor in GPCR trafficking has been suggested[15], it has not been demonstrated.

In this study, we characterize a direct role for myosin VI in the temporal profile of GPCR signaling and advance mechanistic insights into PDZ adaptor regulation of GPCRs. Our results demonstrate that myosin VI activity is critical for D2R trafficking and signaling. We find that PBM sequence information in the GPCR C-tail is differentially decoded by myosin VI, resulting in varied motor activity. We report an interaction between the D2R C-tail and the third intracellular loop that regulates both ligand efficacy and contextual factors in receptor trafficking. Together, our study advances a conceptual framework for differential cytoskeletal regulation of GPCR trafficking and signaling.

Results

Myosin VI activity is necessary for agonist-stimulated D2R internalization

D2R has previously been shown to interact with GIPC through a PDZ motif (type III) in its C-tail[12]. While GIPC is known to directly interact with myosin VI[26], and recently shown by our group to stimulate myosin VI activity[23], a direct link between myosin VI and GPCR function has not been established. Nonetheless, myosin VI is uniquely positioned to influence endocytosis as the only minus-end directed actin-based motor[19]. Hence, we used a myosin VI-selective inhibitor (TIP)[27–30] and a GIPC dominant negative (GIPC(ΔMIR)), lacking the myosin VI interacting region (MIR)[23,31], to examine myosin VI function in D2R internalization (Fig. 1a). TIP pretreatment (100 μM; 15 min) or GIPC(ΔMIR) co-expression (verified by TagRFP fusion; Supplementary Fig. 1) inhibited quinpirole (quin; 1 μM)-stimulated D2R internalization, observed using live imaging of antibody labeled D2R in HEK293 cells (Fig. 1a, b; Supplementary Fig. 2, See Methods). TIP and GIPC(ΔMIR) significantly reduced the number of internalized puncta per cell (Fig. 1c, Supplementary Fig. 1B) and cytosol-to-surface ratio of fluorescence intensity (Fig. 1d, Supplementary Fig. 1C). D2R is natively expressed in medium-spiny neurons (MSNs), a major neuronal subtype in the striatum[32]. MSNs overexpressing D2R were stimulated with quin, resulting in significant D2R internalization (Fig. 1e–g). TIP pretreatment abolished quin-stimulated D2R internalization, demonstrating that myosin VI activity is vital in a native environment (Fig. 1f, g). However, GIPC(ΔMIR) did not have a noticeable effect on D2R internalization in MSNs (Supplementary Fig. 1D), suggesting additional myosin VI coupling through neuron-specific PDZ adaptors[33–35].

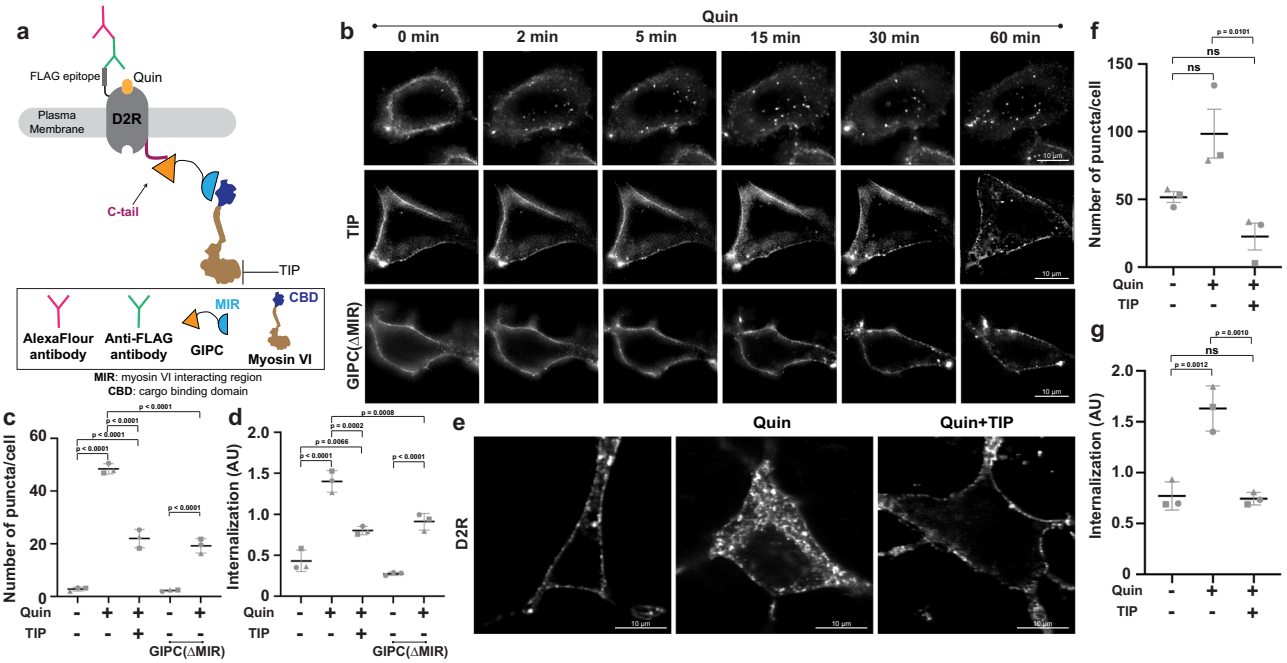

Fig. 1 | Myosin VI engagement and activation are necessary for agonist-stimulated D2R internalization. a Schematic of N-terminal FLAG-tagged D2R bound to M2 anti-FLAG antibody and Alexa 546 secondary. Receptors were tagged similarly for internalization experiments throughout the study, unless indicated otherwise. PDZ binding motif (PBM) in the D2R C-tail engages GIPC, which in turn interacts with myosin VI through a myosin-interacting-region (MIR). TIP inhibits myosin VI catalytic activity, while deletion of the MIR region in GIPC (GIPC(ΔMIR)) is expected to de-couple myosin VI from D2R. **b** Live cell imaging of HEK293 cells expressing D2R following quinpirole (quin; 1 μM) stimulation, in the presence of either TIP (100 μM) or co-expression of GIPC(ΔMIR) (Supplementary Fig. 1A). Scale bar − 10 μm. **c**, **d** Number of puncta per cell **c** and cytosol-to-cell surface intensity **d** (Supplementary Fig. 1B, C; see Methods) under basal or quin-stimulated (1 μM; 60 min) conditions in the presence of TIP (100 μM) or GIPC(ΔMIR) co-expression. Mean +/- SD is indicated along with the average values for three biological replicates (n > 15 cells analyzed for each replicate). Statistical differences were assessed by one-way ANOVA, followed by Tukey's post hoc test. **c**, $F = 219.5$, d.f. = 14; **d**, $F = 60.92$, d.f. = 14. **e** Representative image of medium spiny neurons (MSNs) expressing D2R at basal or quin-stimulated +/- TIP conditions. **f, g** Number of puncta per cell **f** and cytosol-to-cell surface intensity **g** under basal or quin-stimulated conditions in the presence of TIP in MSNs. Mean +/- SEM **f** and mean +/- SD **g** is indicated for three biological replicates (n > 10 cells analyzed for each replicate). Statistical differences were assessed by one-way ANOVA, followed by Tukey's post hoc test. ns, not significant ($p > 0.05$). **f**, $F = 10.14$, d.f. = 8; **g**, $F = 31.79$, d.f. = 8.

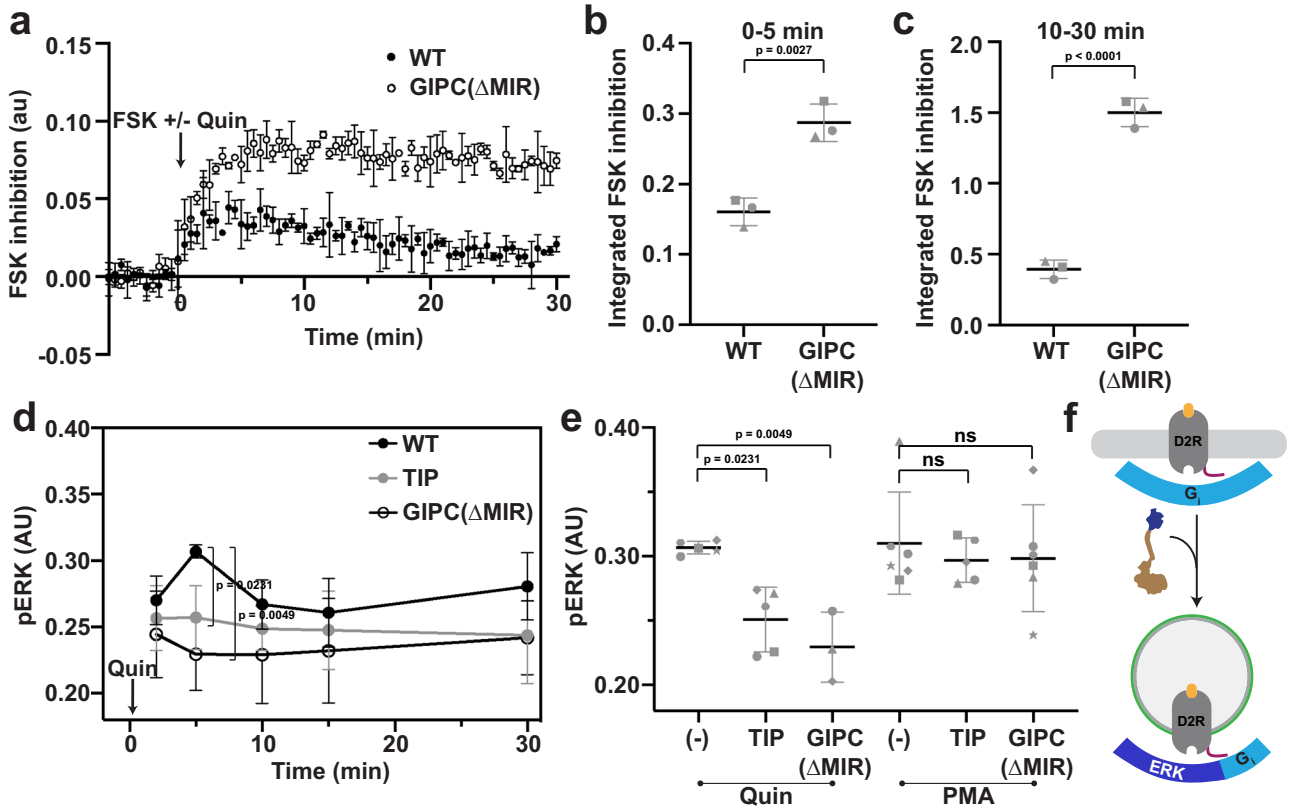

Fig. 2 | Myosin VI influences D2R-mediated G-protein and MAPK signaling. **a** Inhibition of forskolin (FSK; 10 μM) stimulated cAMP in HEK293ΔG$_s$ cells expressing wild-type (WT) D2R or co-expression of D2R with GIPC(ΔMIR) upon quin (1 μM) treatment. cAMP levels were determined as normalized change in fluorescence, post stimulation [(F-F$_0$)/F$_0$]. FSK inhibition was calculated as cAMP signal for FSK+quin treated cells subtracted from cells treated only with FSK (Supplementary Fig. 3A, B). **b**, **c** Area under the curve for 0–5 min **b** and 10-30 min **c** FSK inhibition data in (**a**). **a**–**c** Mean +/- SD is reported for three biological replicates. Statistical differences were assessed by unpaired two-tailed t-test. **b** $t = 6.593$, d.f. = 4; **c**, $t = 16.16$, d.f. = 4. **d** pERK signaling profile in HEK293 cells expressing WT D2R, TIP (10 μM) treatment, or GIPC(ΔMIR) co-expression upon quin (1 μM) stimulation. PMA (3 μM) stimulation was used as a positive control of pERK (Supplementary Fig. 3D). **e** Comparison of pERK signal at 5 min for quin or PMA-stimulated cells. **d**, **e** Mean +/- SD is reported for three-to-six biological replicates. Statistical differences were assessed by one-way ANOVA, followed by Tukey's post hoc test. ns, not significant ($p > 0.05$). **d**, **e** $F = 6.053$, d.f. = 27. **f** Schematic diagram illustrating the role of myosin VI in shaping spatiotemporal D2R signaling. Inhibition of myosin VI leads to elevated and persistent G$_i$ signaling from the cell membrane. pERK signaling from internalized compartments is also dependent on myosin VI activity.

Myosin VI influences the temporal profile of D2R signaling

D2R is a canonical G$_i$-coupled receptor that suppresses cAMP levels[32,36] and stimulates ERK1/2 activation[37]. To examine the impact of myosin VI activity on D2R signaling, we first examined the temporal profile of D2R-mediated inhibition of FSK-stimulated cAMP accumulation in HEK293 cells overexpressing the receptor (Fig. 2a). Quin stimulation (1 μM) initially suppresses cAMP, with a peak response at 5 min that is subsequently diminished (10-30 min post stimulation; Fig. 2a–c). Co-expression of D2R with GIPC(ΔMIR) significantly enhanced quin-stimulated cAMP inhibition. Notably, GIPC(ΔMIR) prolonged the D2R response, with persistent inhibition detected up to 30 min (Fig. 2a–c; Supplementary Fig. 3A-B). However, the myosin VI inhibitor TIP interfered with cAMP sensor basal fluorescence levels (Supplementary Fig. 3C) and was not evaluated for its effects on cAMP signaling. Quin stimulation transiently enhanced pERK1/2 levels (peak at 5 min; Fig. 2d) in HEK293 cells expressing D2R. GIPC(ΔMIR) co-expression or TIP treatment (10 μM) abolished the pERK1/2 response (Fig. 2d, e). Neither TIP nor GIPC(ΔMIR) influenced PMA-induced pERK1/2 (Supplementary Fig. 3D). Since PMA stimulates Protein Kinase C, which in turn activates ERK1/2[38], these data support a myosin VI-dependent mechanism for quin-stimulated pERK1/2. Together, our data are consistent with D2R mediated G$_i$ signaling from the plasma membrane and ERK1/2 signaling from the internalized receptor (Fig. 2f). Suppressing receptor internalization through myosin VI is sufficient to disrupt pERK1/2, while augmenting G$_i$ signaling presumably through sustained plasma membrane localization.

D2R internalization is β-arrestin-independent

The mechanism of D2R endocytosis is unclear, with dynamin-dependent[39], dynamin-independent[40], and partially dynamin-independent[41] internalization variously reported. A caveat to these studies is their reliance on over-expression of dominant-negative mutant constructs over a period of several days, during which compensation by up-regulation of alternate pathway(s) may occur[42]. As an alternative approach, quin-stimulated internalization of D2R was assessed after acute chemical inhibition imposed by the small-molecule drug Dyngo4a (Dyngo)[43]. Dyngo strongly inhibited D2R internalization measured 60 min after application, suggesting that D2R endocytosis is mediated primarily by a dynamin-dependent pathway (Supplementary Fig. 4).

Dynamin-dependent GPCR endocytosis is traditionally associated with β-arrestin recruitment to the phosphorylated receptor[1,44,45]. However, D2R has a relatively short C-terminus[12] that lacks phosphorylation sites canonically associated with β-arrestin recruitment and signaling[46–48]. Nonetheless, it displays agonist-dependent β-arrestin recruitment, likely through the engagement of its finger loop motif with the cytosolic cavity of the receptor[49]. To assess a requirement for β-arrestin for D2R internalization, quin-stimulated receptor

https://doi.org/10.1038/s41467-024-55053-9

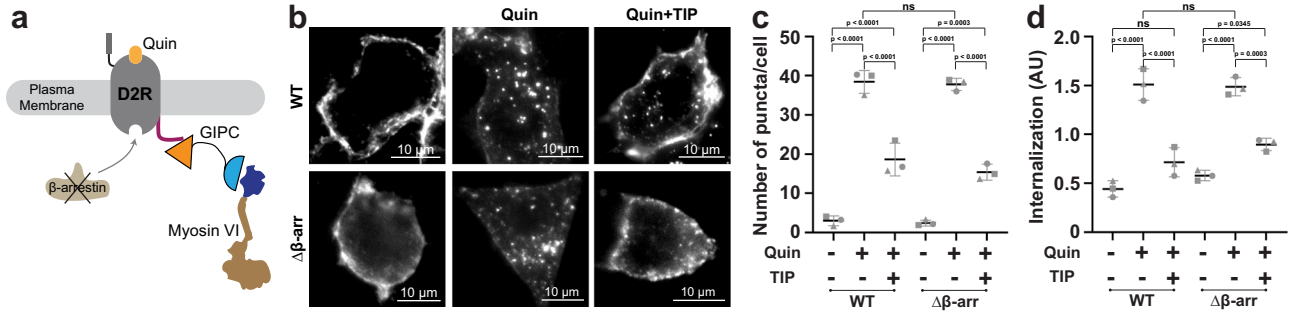

Fig. 3 | D2R internalization is β-arrestin independent. a Schematic representation of D2R internalization independent of β-arrestin. **b** Representative images of D2R internalization in HEK293 WT or HEK293 β-arrestin double knockdown (Δβ-arr) cells upon stimulation with quin (1 μM) and TIP treatment (100 μM) at 60 min. **c**, **d** Number of puncta per cell **c** or cytosol-to-cell surface intensity **d** under basal, quin, and quin+TIP conditions. Mean +/- SD is reported for three biological replicates (n > 10 cells analyzed for each replicate), with statistical significance assessed by one-way ANOVA, followed by Tukey's post hoc test. ns, not significant ($p > 0.05$). **c**, $F = 132$, d.f. = 17; **d**, $F = 53.66$, d.f. = 17. See also Supplementary Figs. 5 and 6.

internalization was monitored in wild-type (WT) and β-arrestin double knock-out (Δβ-arr) HEK293 cells (Fig. 3a, b). Interestingly, Δβ-arr does not block receptor internalization, assessed by the number of puncta per cell (Fig. 3c) and the ratio of cytosol-to-surface fluorescence (Fig. 3d). Likewise, β-arrestin overexpression did not augment quin-stimulated D2R internalization (Supplementary Fig. 5). Pre-treatment of cells with myosin VI inhibitor (TIP; 100 μM) abolishes D2R internalization, both in WT and Δβ-arr cells suggesting that receptor internalization is myosin VI-dependent but β-arrestin-independent. In contrast, consistent with previous reports[50,51], V2R internalization is significantly reduced in Δβ-arr cells (Supplementary Fig. 6). V2R lacks a canonical PDZ-motif at its C-terminus[6] and correspondingly myosin VI inhibition (TIP treatment) did not have significant effect on receptor internalization (Supplementary Fig. 6C, D). Together, our data suggest that D2R endocytosis occurs via a dynamin-mediated pathway that is dependent on myosin VI rather than β-arrestin.

D2R C-tail is sufficient for myosin VI-dependent regulation of GPCR internalization and signaling

D2R has a type III PDZ-binding motif (-LHC)[6] that facilitates GIPC recruitment[12]. To examine sufficiency of the D2R C-tail for myosin VI-mediated GPCR internalization, we investigated a V2 vasopressin receptor (V2R) chimera (Fig. 4a). V2R chimera (V2RΔ-D2R) comprises a C-terminally truncated V2R (V2RΔ)[52,53] fused to the D2R C-tail. V2R agonist, [Arg8]-vasopressin (AVP; 1 μM), treatment stimulates modest V2RΔ internalization that is dramatically enhanced in the V2RΔ-D2R chimera (Fig. 4b, c). V2RΔ-D2R internalization is blocked by the myosin VI inhibitor TIP (100 μM; Fig. 4d, Supplementary Fig. 7A). Disrupting the GIPC-myosin VI interaction with a dominant negative form of either GIPC (GIPC(ΔMIR)) or myosin VI (cargo binding domain - CBD) suppresses V2RΔ-D2R internalization (Fig. 4d, Supplementary Fig. 7A–C). Further, V2RΔ-D2R internalization can be inhibited by a cell penetrating D2R C-tail peptide (Supplementary Fig. 7B, C). Taken together, these data show that disrupting the GPCR-myosin VI complex is sufficient to inhibit agonist-stimulated receptor internalization (Fig. 4d, Supplementary Fig. 7C). The impact of V2RΔ-D2R internalization on receptor signaling was assessed using an enhanced bystander BRET assay (ebBRET; Fig. 4e). V2RΔ activation results in rapid mini$G\alpha_s$ recruitment to the plasma membrane (Fig. 4f), with gradual recruitment to early endosomes (Fig. 4g). V2RΔ-D2R expressed at comparable levels to V2RΔ (Supplementary Fig. 7D) shows reduced mini$G\alpha_s$ recruitment to plasma membrane, consistent with receptor internalization (Fig. 4f). However, V2RΔ-D2R also demonstrates lower recruitment of mini$G\alpha_s$ to early endosomal compartments (Fig. 4h), suggesting that the chimeric receptor has a distinct G protein recruitment profile compared to V2RΔ. Nonetheless, V2RΔ and V2RΔ-D2R show similar sensitivities to AVP concentrations (Fig. 4h), suggesting ligand potencies are preserved between wild-type and chimeric receptors.

D2R C-tail releases myosin VI autoinhibition through GIPC

To address the mechanism of myosin VI-dependent GPCR internalization, we examined the impact of the GPCR C-tail-GIPC complex on myosin VI conformation and activity. Myosin VI exists as an autoinhibited monomer[54] (Fig. 5a). We have previously shown that binding of the isolated GIPC MIR releases myosin VI autoinhibition[23]. The GIPC MIR is occluded in a domain-swapped dimer conformation[31]. Accordingly, full-length GIPC (GIPC FL) does not impact myosin VI conformation measured using a previously reported FRET sensor[23] (Fig. 5a). However, the addition of D2R C-tail to GIPC FL releases myosin VI autoinhibition resulting in diminished FRET (Fig. 5b, Supplementary Fig. 8). The effects of the D2R C-tail on myosin VI activity were determined using an in vitro motility assay (Fig. 5c). While GIPC FL alone has no significant effect on actin gliding speeds, addition of a D2R C-tail peptide enhances motility (~1.5 fold) (Fig. 5d). Hence, the D2R C-tail activates myosin VI through the release of GIPC autoinhibition.

Diverse GPCR C-tails activate myosin VI motility to regulate receptor trafficking

GPCR C-tails contain three distinct PBM subtypes[6]. To understand the influence of distinct PBM sequences on myosin VI activity, we tested the effects of seven isolated GPCR C-tails on in vitro acto-myosin motility (Fig. 5e, f, Supplementary Table 1). The absence of a typical PBM (V2R) yielded no observable effect[6,55], whereas a range of enhanced speeds was observed when the PBM was present (Fig. 5e, f). All three types of PBMs (Fig. 5f; color coded) were capable of augmenting myosin VI speed. The strength of the interaction between GPCR C-tails and the PDZ domain of GIPC was probed using an ELISA binding assay (Fig. 5g). A linear correlation ($R^2 = 0.99$) was observed between binding and myosin VI speed (Fig. 5h, i). Overall, these data suggest that stronger PBM-PDZ interactions facilitate the display of the GIPC MIR[31] resulting in the release of myosin VI autoinhibition and consequent activation.

To examine the sufficiency of the PBM in stimulating myosin VI activity, a previously affinity optimized, minimal PBM (KKETAV)[56] was examined in our motility assays. KKETAV stimulated speeds comparable with VIPR1 suggesting that this optimal PBM is sufficient for GIPC-dependent myosin VI activation (Fig. 5j). To gain insight into the sufficiency of the last five GPCR amino acids in the differential speeds observed, the effect of C-tail chimeric peptides (swapping of the last five amino acids) was investigated (Fig. 5j). The D2R and VIPR1 motifs

https://doi.org/10.1038/s41467-024-55053-9

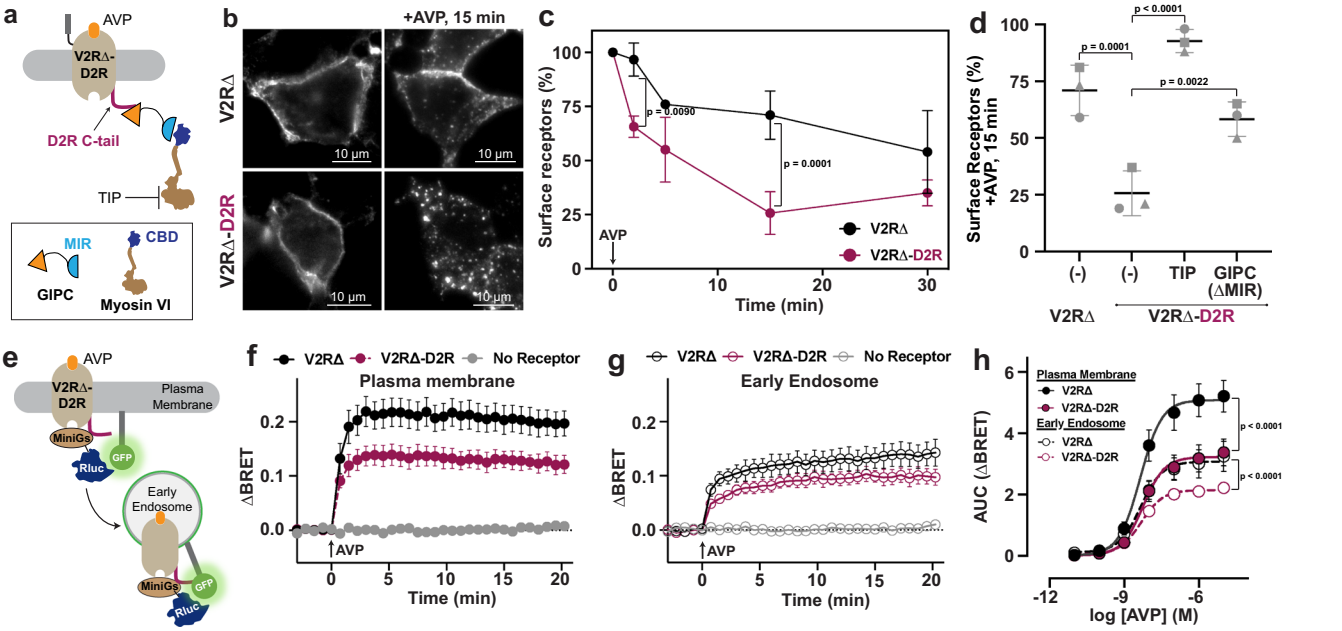

Fig. 4 | D2R C-tail sequence dictates receptor trafficking through recruitment of GIPC-myosin VI. a Schematic of V2R C-tail truncation (V2RΔ) or chimera with D2R C-tail (V2RΔ-D2R). Transposing the D2R C-tail on V2RΔ is designed to recruit the GIPC-myosin VI complex to the chimeric receptor. **b** Representative images of receptor internalization in HEK293 cells expressing V2RΔ or V2RΔ-D2R, stimulated with [Arg8]-vasopressin (AVP; 1 μM) for 15 min. **c** Time-course of surface receptors labeled with anti-FLAG M2 and secondary antibody Alexa 408 in HEK293 cells expressing V2RΔ or V2RΔ-D2R and stimulated with AVP (1 μM). **d** Comparison of level of surface receptors after 15 min agonist stimulation for V2RΔ or V2RΔ-D2R. Cells expressing V2RΔ-D2R were treated with TIP (100 μM) or D2R C-tail (100 μM) or co-expressed with GIPC(ΔMIR) or myosin VI cargo binding domain (CBD) (Supplementary Fig. 7A–C). **c**, **d** Mean +/- SD is reported for three biological replicates, with statistical significance assessed by one-way ANOVA, followed by Dunnett's post hoc test. **c**, **d**, **2 min**, $F = 6.134$, d.f. = 17; **5 min**, $F = 2.273$, d.f. = 17; **15 min**, $F = 20.24$, d.f. = 17; **30 min**, $F = 4.410$, d.f. = 17. **e** Schematic of enhanced bystander bioluminescence resonance energy transfer (ebBRET) assay. MiniGα_s-Rluc8 is recruited to the plasma membrane marker (RGFP-CAAX) or early endosome marker (tdRGFP-Rab5a) upon stimulation of V2RΔ or V2RΔ-D2R with AVP, resulting in an increase in BRET signal. **f**, **g** Recruitment of MiniGα_s to the plasma membrane (CAAX; **f** or the early endosome (Rab5a; **g** in HEK293 cells expressing V2RΔ or V2RΔ-D2R (Supplementary Fig. 7D) at 100 nM AVP. **h** Area under the curve (AUC) for MiniGα_s recruitment to plasma membrane or early endosome at different AVP concentrations. **f**–**h** Mean +/- SEM is reported for five biological replicates, with statistical significance assessed by one-way ANOVA, followed by Tukey's post hoc test. **h**, $F = 219.3$, d.f. = 3999.

swapped into the V2R C-tail enhance myosin VI speeds to D2R levels (Fig. 5j). However, the V2VIPR1 chimeric peptide speed remains significantly lower than VIPR1 alone, suggesting residues upstream of the PBM can influence motility (Fig. 5j).

To test the generality of myosin VI-dependent receptor trafficking, we examined the effect of TIP pretreatment (100 μM; 15 min) on three GPCRs with different PBM subtypes and effects on motility (Fig. 5e, f). Consistent with the enhanced myosin VI motility stimulated by C-tail peptides derived from DOR, LPA1R, and VIPR1 (Fig. 5f), we observe a significant reduction in receptor internalization following TIP treatment for these three receptors (Fig. 5k–m). In contrast, V2R does not stimulate myosin VI motility and correspondingly its internalization is not affected by TIP treatment (Supplementary Fig. 6, Fig. 5k–m).

Myosin VI recruitment is sufficient for shaping GPCR internalization and signaling

To directly examine the role of myosin VI on GPCR trafficking and signaling, we employed a chemogenetic approach[57,58] using rapalog (rapamycin analog) to recruit FKBP (FK506-binding protein)-tagged processive myosin VI dimers to a V2RΔ receptor fused to FRB (FKBP rapamycin binding) at its C-terminus (Fig. 6a). Agonist (AVP) stimulation provides modest V2RΔ-FRB internalization that is significantly enhanced upon rapalog treatment (Fig. 6a, b). Rapalog treatment with agonist results in a greater number of puncta per cell (Fig. 6c) and cytosol-to-cell surface ratio of V2RΔ-FRB (Fig. 6d). Interestingly, rapalog treatment alone is sufficient to stimulate V2RΔ-FRB internalization comparable with agonist treatment (Fig. 6c, d). The enhanced V2RΔ-FRB internalization with rapalog stimulation is accompanied by a significant reduction in cAMP signaling downstream of this canonically G_s-coupled receptor (Fig. 6e). Both the peak response to AVP (Fig. 6f) and sustained signaling (Fig. 6g) are significantly decreased. These data are consistent with our observations for D2R, wherein receptor internalization suppresses plasma membrane G protein signaling (Fig. 2a–c).

GIPC recruitment to D2R C-tail is autoregulated by interactions with ICL3

To examine the agonist dependence of myosin VI activation, we compared internalization profiles of selective D2R agonist quin[39,40], endogenous ligand dopamine (dopa)[10], and selective D2R partial agonist aripiprazole (apz)[59]. We find that dopa and quin have similar endocytic profiles (Supplementary Fig. 6, Supplementary Table 2), whereas apz shows minimal D2R internalization (Fig. 7a–c, Supplementary Table 2). Given our findings of the GIPC-myosin VI complex (Figs. 1, 4), we hypothesized that apz internalization is limited by ligand-dependent GIPC engagement and consequently myosin VI activation. Supporting this hypothesis, we find that GIPC overexpression rescues apz-stimulated D2R internalization (Fig. 7a–c, Supplementary Table 2), without measurably augmenting the effects of dopa or quin (Supplementary Fig. 9, Supplementary Table 2).

GIPC binds the GPCR C-tail, which has been recently shown to engage in autoregulatory interactions with the receptor cytosolic cavity in β2AR[60]. While D2R has a relatively short C-terminus, it has a longer third intracellular loop (ICL3 – 134 aa) that also participates in

https://doi.org/10.1038/s41467-024-55053-9

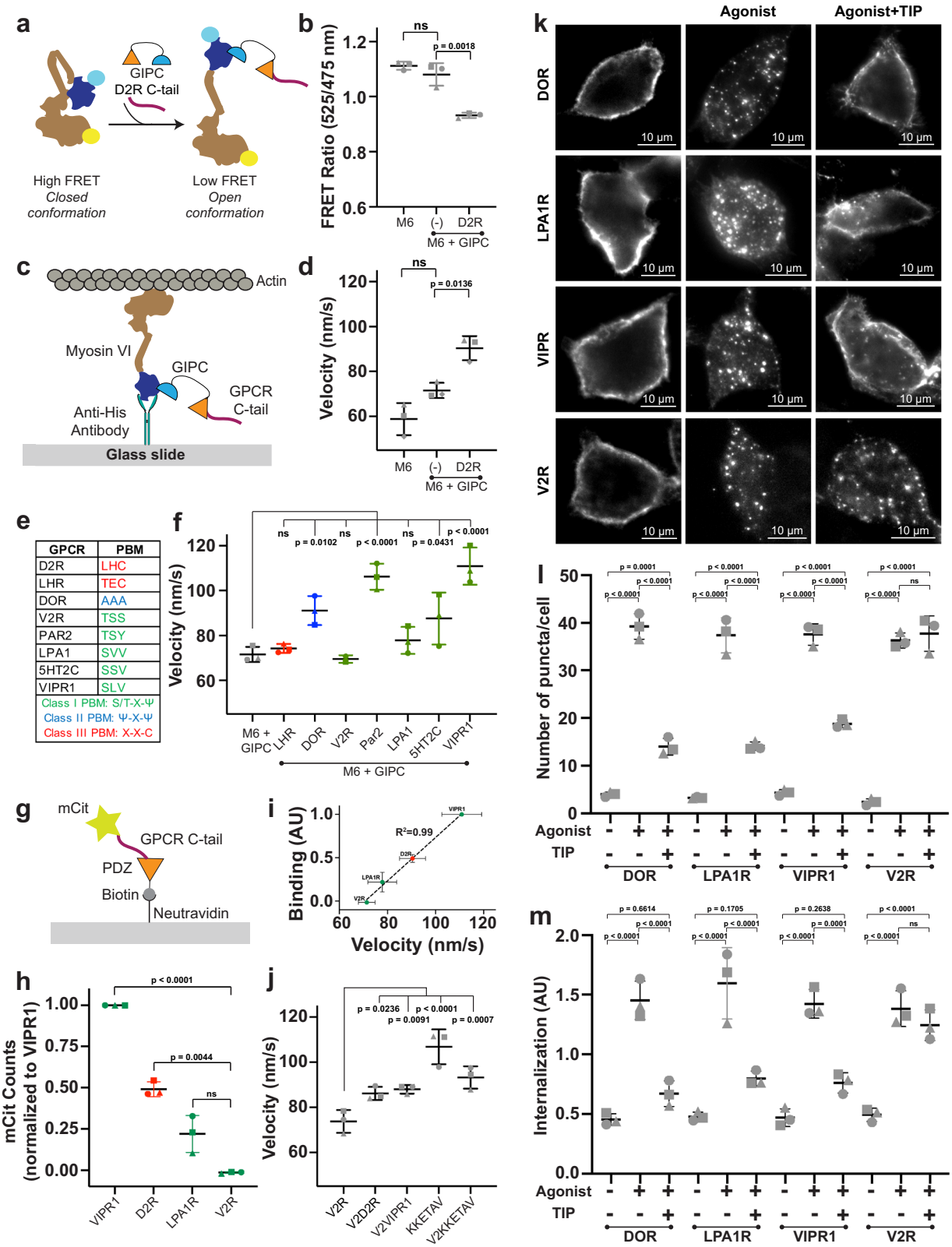

basal autoregulation by gating access to the cytosolic cavity[61]. Hence, we reasoned that GIPC access to the D2R C-tail is limited by intramolecular interactions with ICL3. To probe for such an interaction, we developed a SPASM FRET sensor comprising the isolated D2R C-tail and ICL3, presented as a 'loop', using anti-parallel coiled-coil domains. The FRET ratio of SPASM sensors correlates linearly with the strength of the interaction between protein/peptides at each end of the ER/K linker[62] (Fig. 7d). We find that the sensor reports a significant interaction between the D2R ICL3 and C-tail peptide, while no measurable interaction is observed with a sequence-scrambled C-tail control (Fig. 7e). To investigate a functional role for this interaction, we assessed D2R internalization in an ICL3 deletion mutant (D2R(ΔICL3)). While no significant effects on internalization were observed for full agonist quin (Supplementary Fig. 9, Supplementary Table 2), dopa-

https://doi.org/10.1038/s41467-024-55053-9

Fig. 5 | Myosin VI activity is differentially regulated by PDZ-binding motif (PBM) of GPCRs. a Schematic representation of intramolecular FRET sensor for detection of a conformational change in myosin VI (M6). Activation of M6 is indicated by an open conformation (lower FRET). **b** FRET ratio for intramolecular M6 sensor with GIPC (2 μM) and D2R C-tail (100 μM) (Supplementary Fig. 8). **c** Schematic diagram of actin gliding assay to assess M6 motility. **d** Motility speed for M6 with GIPC (2 μM) and D2R C-tail (100 μM). **e** PBM sequences for GPCR C-tails used in motility assay, color-coded based on PBM class. Refer to Supplementary Table 1 for full sequence of GPCR C-tails used in motility assay. **f** Motility speed of M6 with GIPC and different GPCR C-tails (100 μM). **b**, **d**, **f** Mean +/- SD is reported for three biological replicates, with statistical significance computed by one-way ANOVA, followed by Dunnett's post hoc test. ns, not significant ($p > 0.05$). **b**, $F = 14.28$, d.f. = 9; **d**, **f**, $F = 18.98$, d.f. = 29. **g** Schematic for ELISA assay for biotinylated PDZ1 domain of GIPC binding to mCitrine (mCit)-GPCR C-tails. **h** Binding of GPCR C-tails (D2R, LPA1R, and V2R normalized to VIPR1) to PDZ1 at matching concentration (100 nM). Mean +/- SD is reported for three biological replicates, with statistical significance computed by one-way ANOVA, followed by Dunnett's post hoc test. $F = 160.4$, d.f. = 9. **i** Motile speeds for M6 in the presence of GIPC and indicated GPCR C-tails plotted against mCit counts from the ELISA assay. Mean +/- SD is reported for three biological replicates. Simple linear regression was fit to the data to obtain the R^2 value. **j** M6 motility with GIPC and chimeric GPCR C-tails and affinity optimized KKETAV. Mean +/- SD is reported for three biological replicates, with statistical significance computed by one-way ANOVA, followed by Dunnett's post hoc test. ns, not significant ($p > 0.05$). $F = 59.10$, d.f. = 20. **k** Representative images of DOR, LPA1R, VIPR1, and V2R internalization in HEK293 WT cells upon stimulation with respective agonists (1 μM DPDPE, 10 μM LPA, 500 nM VIP, and 1 μM AVP) for 15 min (VIPR1 and V2R) or 30 min (DOR and LPA1R). Myosin VI activity was inhibited by TIP treatment (100 μM). **l**, **m** Number of puncta per cell **l** or cytosol-to-cell surface intensity **m** under basal, agonist, and agonist+TIP conditions. Mean +/- SD is reported for three biological replicates (n > 10 cells analyzed for each replicate), with statistical significance assessed by one-way ANOVA, followed by Tukey's post hoc test. ns, not significant ($p > 0.05$). **l**, $F = 186.9$, d.f. = 35; **m**, $F = 35.38$, d.f. = 35.

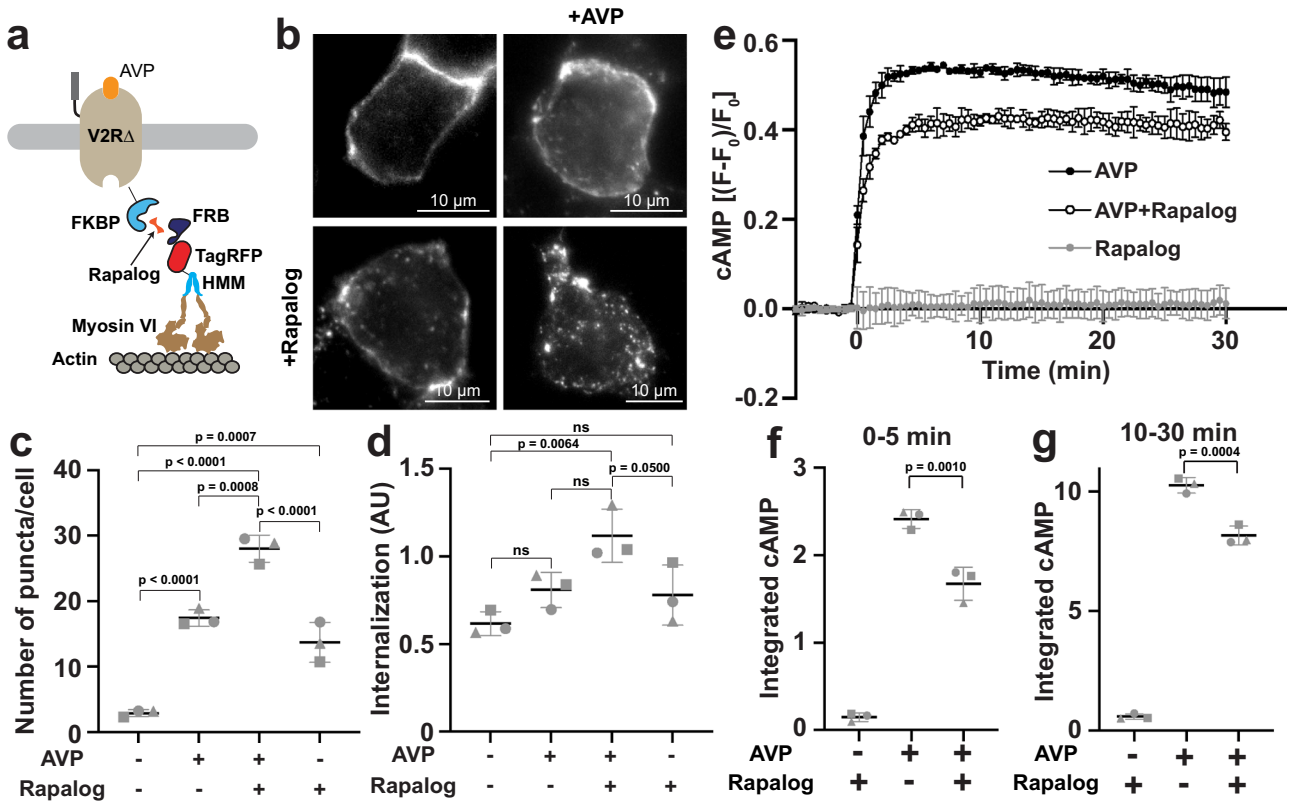

Fig. 6 | Direct recruitment of myosin VI drives trafficking and signaling of GPCRs. a Schematic illustration of chemogenetic recruitment of constitutively active M6 heavy meromyosin (HMM) dimer to V2RΔ. Rapalog addition induces recruitment of M6-FRB (FKBP rapamycin binding) to V2RΔ-FKBP (FK506-binding protein). **b** Internalization of V2RΔ in HEK293 cells upon recruitment of M6. **c**, **d** Number of puncta per cell **c** and cytosol-to-cell surface intensity **d** under basal or AVP stimulation (1 μM; 15 min) conditions +/- rapalog (1 μM). Cells with similar fluorescence intensity level of M6 were quantified. Mean +/- SD is reported for three biological replicates, with statistical significance computed by one-way ANOVA, followed by Tukey's post hoc test. ns, not significant ($p > 0.05$). **c**, $F = 83.29$, d.f. = 11; **d**, $F = 7.84$, d.f. = 11. **e** cAMP levels over time upon agonist stimulation (100 nM AVP) and rapalog (1 μM)-mediated recruitment of M6 to V2RΔ. cAMP levels were assessed using an increase in fluorescence intensity for cADDis biosensor, normalized to initial fluorescence baseline. **f**, **g** Area under the curve for 0-5 min **f** and 10–30 min **g** cAMP levels. **e**–**g** Mean +/- SD is reported for three biological replicates, with statistical significance computed by one-way ANOVA, followed by Tukey's post hoc test. **f**, $F = 241.0$, d.f. = 8; **g**, $F = 846.0$, d.f. = 8.

and apz-stimulated internalization were enhanced (Fig. 7f–h, Supplementary Table 2). D2R is expressed as two distinct splice variants, with distinct lengths of ICL3 (a long variant, D2LR – referred to as D2R in this study, and D2SR; see Methods). We observe similar internalization profiles for both D2R and D2SR in response to quin, dopa, and apz (Supplementary Fig. 10). Consistent with an identical C-tail sequence in both isoforms, GIPC overexpression enhances apz but not quin or dopa-stimulated D2SR internalization.

Contextual regulation of D2R trafficking by myosin VI

Our findings suggest that proteins that interface with either the D2R C-tail or ICL3 can modulate GIPC binding and consequently myosin VI-dependent trafficking. NCAM is a glycoprotein that has been demonstrated to bind the D2R ICL3 and enhance D2R internalization[63]. To test for contextual effects of NCAM, cells were pretreated with a cell permeable NCAM peptide (NCAMp) whose sequence is part of the binding interface between NCAM and D2R

https://doi.org/10.1038/s41467-024-55053-9

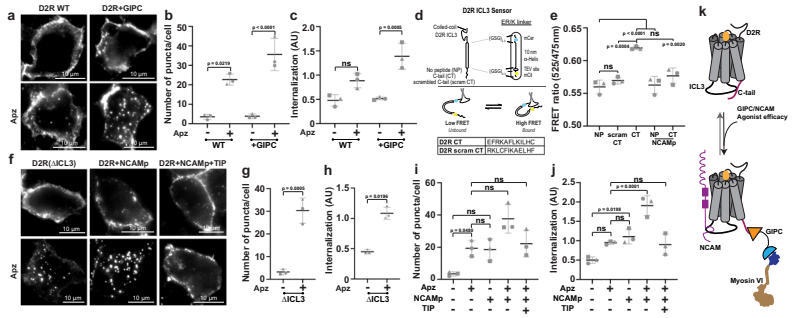

Fig. 7 | Myosin VI decodes receptor autoregulation and agonist trafficking. **a** Representative images of D2R internalization in HEK293 cells upon aripiprazole (apz; 1 μM) stimulation at 60 min, with or without GIPC co-expression. **b**, **c** Number of puncta per cell **b** or cytosol-to-cell surface intensity **c** under basal or agonist stimulation for D2R +/- GIPC co-expression (Supplementary Figs. 9 and 10, Supplementary Table 2). **d** Schematic diagram of D2R ICL3 FRET sensors with no peptide (NP), D2R C-tail (CT), or scrambled CT. NCAM peptide (NCAMp) was added at 50 μM to NP or CT sensors. **e** FRET ratio of ICL3 sensors. **f** Internalization, 60 min post apz stimulation, for D2R(ΔICL3), D2R with NCAMp (30 μM) with or without TIP treatment (100 μM). **g**–**j** Number of puncta per cell **g**, **i** or cytosol-to-cell surface intensity **h**, **j** under basal or agonist stimulation for conditions in **f** (Supplementary Figs. 9, 11A–C, Supplementary Table 2). Mean +/- SD is indicated along with the average values for three biological replicates (n > 15 cells analyzed for each replicate). Statistical differences were assessed by one-way ANOVA, followed by Tukey's post hoc test. ns, not significant ($p > 0.05$). **b**, $F = 22.11$, d.f. = 23; **c**, $F = 24.05$, d.f. = 23; **e**, $F = 21.39$, d.f. = 16; **g**, $F = 49.69$, d.f. = 11; **h**, $F = 31.89$, d.f. = 11; **i**, $F = 12.74$, d.f. = 32; **j**, $F = 32.18$, d.f. = 32. **k** Schematic representation for ICL3-CT autoregulation of GPCR, mediated by agonist, contextual effector proteins, and myosin VI.

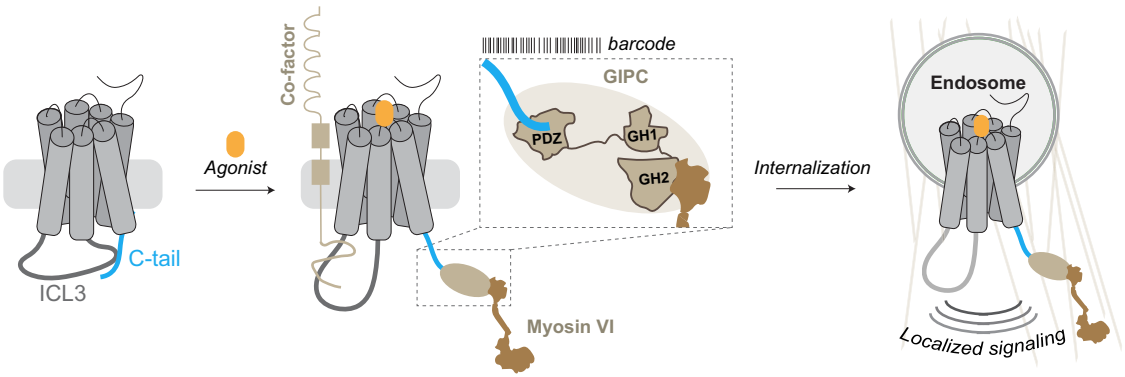

Fig. 8 | Myosin VI shapes internalization and signaling profile of GPCRs. Model schematic demonstrating myosin VI-mediated internalization and signaling of GPCRs. Receptors with distinct PBMs in their C-tail serve as a barcode for recruitment of myosin VI through a PDZ-containing adaptor (GIPC). Agonist stimulation results in release of ICL3 and C-tail autoregulatory interaction, allowing recruitment of co-factor and GIPC-myosin VI complex. GIPC binds to the PBM of GPCRs through the PDZ domain and to myosin VI through the GH2 domain. Recruitment of GIPC-myosin VI complex to the GPCR enhances receptor internalization and mediates localized signaling.

ICL3[63]. NCAMp is sufficient to quench the interaction between the D2R C-tail and ICL3 in the SPASM FRET sensor (Fig. 7e). This release of C-tail regulation correlates with NCAMp pretreatment substantially augmenting apz-stimulated D2R internalization, similar to the levels of full agonists quin and dopa (Fig. 7f, i, j; Supplementary Fig. 11a–c). Furthermore, TIP pretreatment abolishes the effect of NCAMp on apz-stimulated D2R internalization (Fig. 7f, i, j, suggesting that the release of autoregulation facilitates myosin VI recruitment.

Discussion

Our study delineates a β-arrestin-independent mechanism for decoding agonist trafficking of multiple GPCRs through the differential engagement and activation of a cytoskeletal motor, myosin VI. We propose a model wherein agonist activation of the receptor releases autoregulatory interactions involving the C-tail and third intracellular loop (Fig. 8; Supplementary Fig. 11D). The PBM sequence on the GPCR C-tail subsequently engages GIPC, a PDZ adaptor protein. PBM-GIPC interactions reveal the myosin interacting region (MIR) that in turn releases myosin VI autoinhibition to stimulate receptor accumulation on endosomes. Endosomal trafficking stimulated by myosin VI blunts G protein signaling at the plasma membrane while activating ERK1/2 phosphorylation on endosomal compartments. A range of GPCR PBMs differentially activate myosin VI, providing an adaptive mechanism to modulate endosomal trafficking.

Myosin VI has been shown to play a role in trafficking of cell surface receptors, including PlexinD1, megalin, TrkA/B, NMDA, and AMPA[24,25,30,31,34,64–66]. The functional diversity of myosin VI correlates with its role in a range of disease states. Loss of myosin VI function results in chronic physiological defects (*Snell's waltzer* mouse)[67,68], including deafness, proteinuria, and hypertrophic cardiomyopathy[69–71]. Myosin VI overexpression is associated with enhanced cell migration in multiple cancers[20,22]. Nonetheless, a direct link between myosin VI and trafficking of members of the GPCR superfamily has not been demonstrated and is systematically dissected in this study.

Myosin VI is the only minus-end directed actin-based motor[21,54]. The polarity of the actin cortical region, with minus-ends pointed towards the cell interior, enables myosin VI-driven vesicle motion away from the plasma membrane[19,22,33]. As such, myosin VI is uniquely positioned as a cytoskeletal motor to regulate the desensitization and endocytosis of receptors from the actin-rich periplasmic space. Correspondingly, we observe that inhibition of myosin VI leads to receptors lingering in endosomes near the plasma membrane (Figs. 1, 7).

Myosin VI achieves multi-functionality by pairing with various adaptors (Dab2, GIPC, Tom1/2, LMTK2)[20], allowing the motor to regulate different stages of the endocytic cascade. Our study focuses on

GIPC, a myosin VI adaptor that has previously been shown to localize to uncoated vesicles[17]. GIPC-myosin VI interactions in the actin-rich periplasmic space are proposed to facilitate timely endocytosis[18]. While we focus on GIPC as a PDZ adaptor in the early endocytic cascade in HEK293 cells, previous studies have also demonstrated other PDZ adaptors, that operate in specialized cellular contexts (PSD-95 and SAP97 in synaptosomes), as potential myosin VI adaptors[33–35]. Further, the myosin VI interactome intersects with endocytic adaptors previously implicated in GPCR trafficking[72]. Hence, while myosin VI inhibition with the ATPase inhibitor TIP neutralizes receptor endocytosis in our assays, dominant negative GIPC mutants have comparatively moderate (Figs. 1, 2) to insignificant effects (Supplementary Fig. 1D) in parallel assays. Nonetheless, the myosin VI inhibitor does not affect endocytosis of V2R (Supplementary Fig. 6), which lacks the canonical PDZ motif[6] and does not stimulate myosin VI motility (Fig. 5f). Hence, while our study is focused on GIPC, our conceptual insights have broader implications for the myosin VI-dependent regulation of GPCRs.

We discover that the strength of the interaction between the PDZ domain and GPCR C-tail linearly correlates with myosin VI activity (Fig. 5i). Further, the sequence-optimized high affinity PBM (KKETAV)[56] resulted in the largest increase in myosin VI motility (~ 1.8 fold; Fig. 5j). However, in addition to the PBM sequence, our data suggest that PBM effects on myosin VI are contextual to entire GPCR C-terminus. While introducing a high affinity PBM is sufficient to enhance myosin VI motility (V2D2R vs V2R; Fig. 5j), sequence information upstream of the PBM also contributes to myosin VI activity. Specifically, while V2D2R matches the speed of D2R, V2VIPR1 is slower than VIPR1.

We find that myosin VI-facilitated D2R internalization is independent of β-arrestin. D2R has a short C-tail that lacks the extensive phosphorylation sites typically associated with GRK phosphorylation and subsequent β-arrestin recruitment[47]. Further, β-arrestin1/2 knockout does not affect D2R internalization (Fig. 3). However, myosin VI inhibition in a β-arrestin null background is sufficient to block internalization. Hence, our study highlights a β-arrestin-independent mechanism that progresses through PBMs engagement of cytoskeletal motors. Given the differential activation of myosin VI by distinct GPCR C-tails, we propose that the GPCR PBM parallels the previously demonstrated C-terminal β-arrestin barcode[47] that differentially engages and regulates receptor trafficking and signaling (Fig. 8; Supplementary Fig. 11D). While D2R internalization is not dependent on β-arrestin, we speculate that GPCRs with both PBMs and GRK phosphorylation sites may engage synergies between β-arrestin and myosin VI dependent mechanisms.

We propose a structural mechanism that decodes agonist efficacy to regulate GPCR trafficking (Fig. 8). Recent studies using β2AR have independently demonstrated autoregulatory interactions between the effector binding cytosolic cavity of the receptor and either its ICL3[61] or C-tail[60]. Here, we demonstrate a direct, specific interaction between the D2R ICL3 and C-tail that regulates GIPC binding and consequent myosin VI-dependent trafficking. Contextual factors that modulate this interaction, including agonist efficacy, GIPC overexpression, and proteins that interface with ICL3 (e. g. NCAM)[63], regulate myosin VI engagement and consequently the extent of D2R trafficking. Hence, rather than function as a binary 'on-off' mechanism, our data show that myosin VI decodes agonist efficacy and contextual factors to tune receptor trafficking and signaling. Given the widespread use of apz in the treatment of neuropsychiatric disorders[59,73,74], our study provides a mechanism for the cellular actions of GPCR therapeutics through the cytoskeletal regulation of agonist trafficking. We propose that the sequence diversity of GPCR PBMs and ICL3, a range of myosin VI-binding PDZ adaptors, and modulation of myosin VI and adaptor expression in disease states such as cancer, provide opportunities for contextual therapeutics.

Methods

Ethics statement

All procedures were performed according to the National Institutes of Health Guide for Care and Use of Laboratory Animals and approved by the UCSF Institutional Animal Care and Use Committee (protocol number AN185688).

Cell culture

HEK293T Flp-In T-Rex cells (ATCC, referred to as HEK293 cells elsewhere in the manuscript) were cultured in complete Dublecco's modified eagle medium (DMEM, Life Technologies) supplemented with 10% fetal bovine serum (FBS, GenClone), GlutaMAX (Thermo Fisher), and 20 mM HEPES (Corning) at 37 °C with 5% CO_2. Cells were maintained in 10 cm tissue-culture plates and split every 3-4 days (at 85–90% confluency). HEK293 G-protein knockdown cells (ΔGs/olf/q/11/12/13, referred to as HEK293 ΔG_s cells[75]) were maintained in DMEM supplemented with 10% FBS, 20 mM HEPES, GlutaMAX, and penstrep (Life Technologies) at 37 °C and 5% CO_2. HEK293 β-arrestin 1/2 knockdown cells (referred to as HEK293 Δβ-arr cells[76]) were maintained in DMEM supplemented with 10% FBS, 20 mM HEPES, GlutaMAX at 37 °C and 5% CO_2. *Spodoptera frugiperda* insect cells (Thermo Fisher, referred to as Sf9 cells) were cultured in Sf900-II media (Life Technologies) supplemented with antibiotic-antimycotic (Life Technologies) at 28 °C. Cells were routinely passaged every 3-4 days.

Primary rat striatal neuron culture

Medium spiny neurons were prepared from embryonic day 18 Sprague-Dawley rats. After euthanasia of the pregnant Sprague-Dawley rat (CO_2 and bilateral thoracotomy), the brains of embryonic day 18 rats of both sexes were extracted from the skull. The striatum, including the caudate-putamen and nucleus accumbens, was dissected in ice cold HBSS calcium/magnesium/phenol red free (Thermo Fisher). Structures were dissociated in 0.05% trypsin/EDTA (UCSF Media Production) for 15 min at 37 °C and washed in DMEM (Thermo Fisher) supplemented with 10% fetal bovine serum (UCSF Media Production) and 30 mM HEPES. Cells were then mechanically separated with a flame-polished Pasteur pipette and were plated onto poly-D-lysine coated 35 mm glass bottom dishes (Cellvis) in DMEM supplemented with 10% fetal bovine serum. Medium was exchanged on DIV 4-5 for phenol-free Neurobasal medium (Thermo Fisher) supplemented with GlutaMAX 1x (Thermo Fisher) and Gibco B-27 1x (Thermo Fisher). Transfection using Lipofectamine 2000 (Thermo Fisher) was performed on DIV 8 using 2 µl of Lipofectamine and 1-2 µg DNA in 1 ml of media per 35 mm imaging dish. Media was exchanged 4-6 hours later and cytosine arabinosine 2 µM (Millipore Sigma) was added. Cells were maintained in a humidified incubator with 5% CO_2 at 37 °C and imaged at DIV 11-12.

Plasmid construction

Human D2R (long isoform), human D2SR (short isoform), human V2R, human VIPR1, human LPA1R, human DOR, and human GIPC1 (referred as GIPC elsewhere) were cloned into pcDNA5/FRT vector using standard cloning protocols. For all GPCR plasmids, FLAG epitope and mNeonGreen (mNG) tag was included at the N-terminus of the receptor. For dark version of the receptors, only FLAG epitope was included at the N-terminus of the receptor. Deletion of ICL3 in D2R (Δ227-361 residues) was carried out by overlap-extension PCR and the PCR fragment was cloned into pcDNA vector with FLAG and mNeonGreen tag. V2RΔ, V2R C-tail truncation (Δ346-371 residues), was generated by PCR and cloned into pcDNA vector with FLAG +/- mNG tag. V2RΔ-D2R chimera was generated by inserting D2R C-tail using BsmBI-v2 sites in V2RΔ plasmid. FK506-binding (FKBP12) domain was cloned after V2RΔ to generate FLAG-mNG-V2RΔ-FKBP12 or FLAG-V2RΔ-FKBP12. Myosin VI (M6) HMM-GCN4-tagRFP-FRB contains the motor and lever arm domain of human M6 (1-984), followed by GCN4 leucine

zipper, tagRFP, and FKBP rapamycin domain (FRB) and was cloned by replacing GFP with tagRFP[57]. GIPC(ΔMIR) was generated by deleting the myosin interacting region (MIR) with overlapping primers.

MiniGα proteins are truncated Gα proteins that bind to the active conformations of GPCRs[77]. MiniGα_s was tagged on its N-terminus with *Renilla* luciferase (Rluc8)[78] using standard cloning protocol. Subcellular markers for the plasma membrane (prenylation CAAX box of KRas) or early endosomes (Rab5a) tagged with *Renilla* Green Fluorescent Protein (RGFP) were obtained from M. Bouvier (Université de Montréal).

Full length M6 (M6-pBiex), M6 conformation sensor (mCer-M6-mCit-pBiex), M6 CBD-mCer-pBiex, GIPC-mCit-pBiex, and GIPC-pBiex were prepared as previously described[23]. For D2R ICL3 SPASM sensor (p66α-D2R ICL3-MBD2-mCer-mCit) were cloned into pBiex1 backbone following standard cloning procedures. D2R ICL3 region (227-361 residues) was included with antiparallel coiled-coil domains (p66α-MBD2)[79] on either end. No peptide (NP), D2R C-tail (CT), or D2R scrambled C-tail (Scram CT) was cloned after the mCit region for D2R ICL3 SPASM sensor.

Human PDZ1 domain (residues 133-213 of human GIPC1) with His6X, SNAP, and Flag and tags (at N-terminus of PDZ1) were cloned into pET15b vector following standard cloning approach. Standard cloning method was employed to generate Flag-mCitrine-tagged GPCR C-tails (VIPR1 438-547, LPA1R 336-364, D2R 432-443, and V2R 345-371) in pBiex1 vector backbone.

Immunostaining and imaging of striatal neurons

For surface labeling of receptor, neurons were incubated on DIV 11-12 with Alexa Fluor 488-conjugated M1 anti-FLAG antibody (Millipore Sigma, F3040) in pre-equilibrated HEPES buffered saline (HBS) solution (NaCl 120 mM, KCl 2 mM, $MgCl_2$ 2 mM, $CaCl_2$ 2 mM, glucose 5 mM, HEPES 10 mM adjusted to pH 7.4) for 15 min at 37 °C. For the TIP experiment, DMSO or TIP 100 µM was added together with the A488-conjugated M1 anti-FLAG antibody. After two washes with HBS, cells were incubated for 30 min with quinpirole (1 µM), optionally with DMSO or TIP (100 µM), in HBS at 37 °C. Neurons were then fixed with 4% paraformaldehyde and 4% sucrose for 10 min at room temperature, and then washed 3 times with PBS. Neurons were imaged by confocal microscopy using a Nikon Ti inverted microscope equipped with a Yokogawa CSU-22 spinning disk unit, a Photometrics Evolve Delta EMCCD camera controlled by NIS-Elements 5.21.03 software and 488, 561, and 640 nm Coherent OBIS lasers. Samples were imaged using an Apo TIRF 100x/1.49 NA oil objective (Nikon), and 0.3 µm z-stacks were acquired. Quantitative image analysis was performed on unprocessed 16-bit files using ImageJ FIJI[80]. Maximum intensity Z-projection images were created, and a ROI was drawn around the transfected cell. To identify puncta, a binary mask was generated using the "Clear Outside" and "Threshold" commands, with a threshold set manually. Then, the number of internal particles were quantified using the Analyze Particles command, with a minimal pixel size of 0.15 and a circularity of 0.4-1.00.

Internalization assay

HEK293 or HEK293 Δβ-arr cells were seeded on glass coverslips in 35-mm plates (GenClone). The following day, mixture containing DNA and polyethylenimine (PEI; PolySciences; 1:3-4 DNA:PEI) in 100 µL opti-MEM media was added to cells for transfection. FLAG-D2R, FLAG-mNG-D2R, FLAG-mNG-D2R(ΔICL3), FLAG-mNG-D2SR were transfected with 0.5–0.7 µg DNA and 2.5 µL PEI for 20 hrs. For co-expression with GIPC(ΔMIR)-tagRFP, GIPC-tagRFP, or β-arrestin1/2-YFP, GIPC or β-arrestin constructs were transfected with 0.7 µg DNA and 2.5 µL PEI for 20 hrs. For co-expression with β-arrestin1/2-YFP, both β-arrestin constructs were transfected at 0.4 µg DNA and 2.5 µL PEI for 20 hrs. Individual expression of β-arrestin1-YFP and β-arrestin2-YFP was confirmed by immunofluorescence. M6 HMM-tagRFP-FRB was transfected at 1 µg with 3 µL PEI for 24 hrs. FLAG-mNG-V2R, FLAG-V2RΔ-FKBP12, FLAG-V2RΔ and FLAG-V2RΔ-D2R were transfected at 0.8 µg and 2–2.5 µL PEI for 20 hrs. FLAG-mNG-DOR, FLAG-mNG-LPA1R, FLAG-mNG-VIPR1 were transfected at 0.7-0.8 µg and 2–2.5 µL PEI for 23 hrs.

Cells were immunostained the next day after transfection. Prior to antibody staining, the cells were blocked with 0.1% BSA in DMEM at 4 °C for ~15 min. For protocol A, primary anti-FLAG M2 antibody (Sigma) and AlexaFluor 488/546/647 labeled secondary antibody (Thermo Fisher) were incubated in DMEM with 0.1% BSA for 60 min at 4 °C to form a complex. Cells were then labeled with pre-incubated primary/secondary antibody complex at 4 °C for 60 min. For protocol B, cells were pre-incubated with just the primary antibody at 4 °C for 60 min. Next, agonist was added to stimulate internalization in DMEM at 37 °C for the indicated time. D2R was stimulated with full agonists quinpirole (quin; Sigma; 1 µM) or dopamine (dopa; Tocris; 1 µM) or partial agonist aripiprazole (apz; Sigma; 1 µM) for 60 min. All V2R receptors were stimulated with [Arg^8]-vasopressin (AVP; Genscript; 1 µM). DOR and LPA1R expressing cells were stimulated with DPDPE (Tocris; 1 µM) and LPA (Cayman; 10 µM), respectively, for 30 min. VIPR1 was stimulated with VIP (Tocris; 500 nM) for 15 min.

For NCAMp, dyngo4a, or TIP treatment, cells were treated 15 minutes prior to agonist addition with NCAMp (30 µM), dyngo (Abcam; 30 µM), or TIP (Sigma; 100 µM) for 15 min. NCAMp contained a cell penetrating TAT sequence (CYGRKKRRQRRRC) attached to the D2R binding sequence of NCAM (VNLCGKAGPGAKGKDMEEG) with a GSG sequence in between. At the end of the experimental time course, cells were fixed in 4% formaldehyde solution in PBS for 10 min at room temperature, followed by washes in PBS. Cells pre-incubated with primary antibody alone were permeabilized (1% TritonX-100; 25 min), incubated with AlexaFluor 546 secondary antibody (20 min at 37 °C), followed by PBS washes. All cell preparations were mounted onto a clean glass slide using Prolong Anti-Fade Mountant (Thermo Fisher). Protocol A is used throughout the manuscript, with a comparison of protocol A and B presented in Supplementary Fig. 2.

After allowing the samples to cure overnight, coverslips were sealed with valap (vaseline/lanolin/paraffin) and samples were processed for imaging on Nikon Eclipse Ti inverted epifluorescence microscope equipped with 100x oil immersion objective (1.4 numerical aperture (NA)) and Evolve EMCCD camera (Photometrics). Images were acquired along the z-plane at 0.6 µm distance and maximum intensity projection (MIP) was created using Fiji. The acquisition parameters were held constant between different samples. Images were analyzed for two internalization matrices (number of particles and cytosol-to-cell membrane intensity) using Fiji. For number of particles, a difference of Gaussian was created for images, set to threshold, and analyze particles function of Fiji was used to obtain a count for number of particles. Cytosol-to-cell intensity was calculated as the ratio between fluorescence intensity of cytosol and the cell membrane. 10-25 cells were analyzed per each biological replicate and ≥ 3 biological replicates were performed for every condition.

Live-cell imaging

HEK293 cells were grown on 45-mm round coverslips in 60-mm plates and transfected with FLAG-mNG-D2R-pcDNA or FLAG-mNG-D2R-pcDNA + 0.7 µg GIPC(ΔMIR)-pcDNA. 20 hrs post-transfection, FLAG-tagged receptor in HEK293 cells were labeled following the procedure described above (under Internalization assay). Next, the coverslip was mounted onto FCS2 chamber (Bioptechs) for live-cell imaging. Cells were maintained in imaging buffer (Hank's Buffered Saline Solution (HBSS), 0.2% glucose, 100 µM ascorbic acid) for the duration of the imaging. Quin (1 µM) in imaging buffer was perfused into the FCS2 chamber. For TIP treatment, 100 µM TIP was included with the agonist. Live events for internalization were recorded on Nikon Eclipse Ti inverted epifluorescence microscope using oil immersion objective (60×1.4 NA) at 1.5x magnification. The microscope was equipped with

Evolve EMCCD camera (Photometrics) and the FCS2 chamber was used to maintain 37 °C temperature.

cAMP assay

Real-time cAMP levels were measured using Green Up cADDis cAMP sensor (Montana Molecular). HEK293 or HEK293 ΔG_s cells were seeded at 30% density in a 6-well plate. For D2R-mediated inhibition of cAMP, HEK293 ΔG_s cells were used to avoid any crosstalk with G_s. Next day, cells were transduced with cADDis BacMam and transfected with 0.7 µg FLAG-D2R + /− 0.7 µg GIPC(ΔMIR)-tagRFP using 5 µL PEI. 0.6 µg FLAG_V2RΔ_FKBP12 with 1.2 µg M6-HMM-tagRFP-FRB was transfected using 5.5 µL X-tremeGENE HP (Sigma). 24 hours post-transfection, cells were harvested in cAMP buffer (135 mM NaCl, 5 mM KCl, 0.4 mM $MgCl_2$, 1.8 mM $CaCl_2$, 5 mM D-glucose, 20 mM HEPES, pH 7.4) and transferred to a black 96-well flat bottom plate (Greiner Bio-One) at 7e5 cells/well density. The 96-well plate was then transferred to a plate reader (Tecan Spark) and fluorescence was recorded for 5 min (excitation 500 nm, emission 530 nm), every 30 sec. Following this baseline read, drug conditions were added, and recording was continued for 30 min. For D2R conditions, 10 µM forskolin (FSK; Sigma) +/− 1 µM quin was added. For M6 + V2RΔ conditions, 100 nM AV*p* + /− 1 µM rapalog ($C_{59}H_{88}N_2O_{12}$; PubChem ID 44576241; Takara) was added. Rapalog only control was also included. Average of 5 min baseline (F_0) was considered as initial fluorescence for each well. cAMP levels were calculated as F_0 subtracted from fluorescence value for each time point, normalized by F_0. 2-3 technical replicates were included for each condition and 3 biological replicates were performed for every experiment.

Phospho-ERK1/2 (pERK) assay

HEK293 cells were seeded in 35-mm plates at 30% density and transfected with 0.7 µg FLAG-mNG-D2R + /− 0.7 µg GIPC(ΔMIR)-tagRFP and 5 µL PEI. About 20 hrs post-transfection and serum starvation, cells were harvested in DMEM and added to an opaque 384-well flat bottom plate (Greiner Bio-One) at 1.4e4 cells/well density and processed for pERK levels using a kit (CisBio) following the manufacturer's instructions. Quin (1 µM) or PMA (EMD Millipore, 3 µM) was added to each well and reaction was stopped at each time point by adding the kit lysis buffer. For TIP treatment, TIP was added at 10 µM along with quin or PMA. After adding lysis buffer, the 384-well plate was incubated at room temperature, shaking at 500 RPM for 30 min. Next, pre-mixed antibody solution was added to each well. After 4-5 hrs, samples were excited at 314 nm and fluorescence emission was recorded at 665 nm and 620 nm in a HTRF-compatible plate reader (Molecular Devices). pERK levels were calculated as the ratio between 665 and 620 nm signals for an individual well. 3–4 technical replicates were included for each condition and at least 3 biological replicates were performed for every experiment.

Cell-surface receptor assay

HEK293 cells were seeded in 35-mm plates with coverslips at 30% density and transfected with 1 µg FLAG-mNG-V2RΔ or 1 µg FLAG-mNG-V2RΔ-D2R and 4 µL PEI. 0.7 µg GIPC(ΔMIR)-tagRFP or 0.7 µg M6-CBD-tagRFP were co-transfected with FLAG-mNG-V2RΔ-D2R, when applicable. 18 hours post-transfection, agonist (1 µM AVP) was added for stimulation. Cells expressing FLAG-mNG-V2RΔ-D2R were pre-treated with TIP (100 µM) or TAT-D2R C-tail peptide (Genscript; 10 µM) for 30 min, prior to AVP stimulation. At each time point, the cells were washed in cold-PBS and cell surface receptors were stained with anti-FLAG M2 antibody (1:200 dilution), followed by Alexa Fluorophore 408 secondary antibody (Thermo Fisher; 1:250 dilution) at 4 °C for 60 min. Post-staining, cells were harvested from the coverslips and fluorescence spectra were measured using a FluoroMax-4 spectrofluorometer (Horiba Scientific) with the following settings: excitation at 401 nm (4 nm bandpass), emission 410–600 nm (4 nm bandpass, 1 nm intervals). Non-specific fluorescence (no primary antibody, only secondary antibody) was used subtracted for each sample. Maximal fluorescence intensity at 517 nm (mNeonGreen emission) was used to qualify cell surface staining. The percentage of each time point relative to t = 0 min was used to calculate internalization. 3 technical replicates were included for each condition and 3 biological replicates were performed for every experiment.

Enhanced bystander bioluminescence resonance energy transfer (ebBRET)

HEK293 cells were plated in white 96-well microplates (100 µl/well). Cells were transfected with either FLAG-V2RΔ or FLAG-V2RΔ-D2R (20 ng/well) after 24 hrs using PEI (Polysciences; 1:6 DNA:PEI) diluted in a 150 mM NaCl solution. To infer signaling from distinct subcellular compartments, ebBRET components were co-transfected to assess the recruitment of Rluc8-miniGα_s (20 ng/well) to RGFP-CAAX (plasma membrane marker, 20 ng/well) or tdRGFP-Rab5a (early endosome marker, 20 ng/well). Following 18 hrs, cells were washed with Hank's Buffered Saline Solution (HBSS) containing 10% HEPES (pH 7.4). Cells were then pre-incubated with the luciferase substrate for 5 min (Prolume Purple coelenterazine, 2.5 µM; NanoLight Technology). Luminescence and fluorescence emissions were then recorded every 45 s in a Synergy Neo2 Microplate reader (BioTek) (donor filter: 410 ± 80 nm, acceptor filter: 515 ± 30 nm. Following 5 baseline reads, increasing concentrations of AVP (Sigma Aldrich) were added. ΔBRET represents the BRET signal in the presence of agonist, minus the BRET signal over time in the presence of vehicle. Fluorescence intensity for non-permeabilized and saponin-permeabilized cells was pooled together to determine the total amount of receptor expressed.

Sf9 protein expression and purification

Proteins used in FRET and motility assays were transiently transfected and purified from Sf9 cells, as described previously[23]. Briefly, Sf9 cells were transfected using Escort IV transfection reagent (Sigma) as per manufacturer's instructions. 72 hours post-transfection, cells were lysed in lysis buffer (20 mM imidazole pH 7.5, 0.5% IGEPAL, 200 mM NaCl, 4 mM $MgCl_2$, 0.5 mM EDTA, 1 mM EGTA, 5 mM DTT, 7% sucrose, 5 µg/ml aprotinin, 5 µg/ml leupeptin, 5 µg/ml PMSF) and centrifuged at 176000 g, 25 min, 4 °C (TLA 100.4 Beckman). The supernatant containing expressed protein was incubated with anti-FLAG M2 affinity resin (Sigma) for 60 min at 4 °C. Next, the resin was washed in wash buffer (20 mM imidazole pH 7.5, 150 mM KCl, 5 mM $MgCl_2$, 1 mM EDTA, 1 mM EGTA, 5 mM DTT, 7% sucrose, 5 µg/ml aprotinin, 5 µg/ml leupeptin, 5 µg/ml PMSF) 3 times to wash off excess protein. Finally, the bound protein was eluted from resin by incubating with FLAG peptide (Sigma) overnight at 4 °C. Next day, the eluted protein was collected. Purification quality control and quantitation was performed via SDS-PAGE or Nanodrop (for proteins with fluorescent tag).

Myosin VI intramolecular FRET assay

M6 conformational FRET sensor (mCer-M6-mCit) and full length GIPC were expressed and purified from Sf9 cells as described above. All FRET readings were recorded in assay buffer (AB; 20 mM imidazole pH 7.5, 25 mM KCl, 4 mM $MgCl_2$, 1 mM EGTA) with 0.1 mg/ml BSA. M6 sensor and GIPC were added in AB at 50 nM and 2 µM concentration, respectively. The mixture also contained 10 µM calmodulin (Sigma), 2 mM ATP (EMD Millipore), 0.5 µM F-actin. Peptide for D2R C-tail was commercially synthesized (GenScript; refer to Supplementary Table 1 for peptide sequence) and added to the solution at varying concentrations. Samples were excited at 430 nm (8-nm bandpass) and spectra was recorded from 450 nm to 650 nm (4-nm bandpass, 1-nm intervals) on a FluoroMax-4 spectrofluorometer (Horiba Scientific). The FRET ratio was computed from intensity values of mCitrine (525 nm) and mCerulean peaks (475 nm).

Myosin VI surface motility assay

All motility assays were carried out at room temperature and the proteins (M6 and GIPC) were purified from Sf9 cells. GPCR C-tails were commercially synthesized (Genscript; refer to Supplementary Table 1 for peptide sequence). Motility assays were carried out as previously described[23]. Briefly, a motility flow chamber was created by sticking collodion-coated coverslips to a glass slide with a double-sided tape. Coverslips were dipped in 2% collodion solution in amyl acetate (Electron Microscopy Sciences) to coat and air dried under a fume hood before preparing flow chamber. Next, anti-his antibody (Qiagen, 0.02 mg/mL) in AB was added to the flow chamber for 4 min at room temperature. Three washes with AB were carried out to wash off the unbound antibody, followed by blocking with BSA in AB for 2 min. Next, M6 (200 nM) with GIPC (2 µM) and GPCR C-tail (100 µM) in AB-BSA was passed through the flow chamber and incubated for 4 min. Unbound protein was washed off with AB-BSA solution and actin motility mix (F-actin labeled with Alexa-647 phalloidin (Invitrogen), 0.6% glucose, 45 µg/ml catalase (EMD Millipore), 25 µg/ml glucose oxidase (EMD Millipore), 2 mM ATP, 1 mM phospho-creatine (Sigma), 0.1 mg/ml creatine phosphokinase (EMD Millipore), supplemented with additional GIPC and GPCR C-tail peptide to maintain assay concentration) was flown to the chamber. Finally, the flow chamber was mounted on the stage and imaged using Nikon Eclipse Ti inverted epifluorescence microscope equipped with an oil immersion objective (100×1.4 NA) and Evolve EMCCD camera (Photometrics) at 1 frame/sec rate for 3 min. Motility data were analyzed using MTrack plugin on Fiji for 25-30 F-actin tracks per each condition. At least 3 biological replicates were performed for each condition.

Bimolecular FRET assay

GIPC-mCit and M6 CBD-mCer were purified from Sf9 cells, as described above. D2R C-tail was commercially synthesized (Genscript; refer to Supplementary Table 1 for peptide sequence) and used at constant concentration (100 µM). Concentration of M6 CBD (30 nM) was held constant, while GIPC was added at varying concentrations. Bimolecular FRET was carried out in AB with 0.1 mg/ml BSA. Emission spectra were recorded as described in the *Myosin VI intramolecular FRET assay* section above. Spectra for GIPC-mCit alone at each concentration was subtracted for each sample. Finally, FRET ratio (525 nm/475 nm) was plotted against GIPC concentration and dose-response curve was fit using GraphPad Prism (10.2.0).

ICL3 FRET sensor

ICL3 FRET sensors were expressed and purified from Sf9 cells. The ICL3 binding region of NCAM (VNLCGKAGPGAKGKDMEEG) was commercially synthesized (Genscript). E3R3 sequence (EEERRR)[81] was attached to this NCAM peptide to enhance peptide solubility. All FRET sensors were added at 30 nM and NCAM peptide was added at 50 µM. Assays were performed and analyzed as described in the *Myosin VI intramolecular FRET assay* section above.

PDZ1 bacterial purification

SNAP-His-PDZ1-pET15b was transformed into competent *Escherichia coli* SHuffle T7 cells (NEB). Secondary cultures expressing this construct in terrific broth were induced with 0.6 mM IPTG when OD_{600} reached 1.0 at 25 °C for 4 hours or 14 °C for 16 hours. Cells were harvested via centrifugation at 3200 g, 15 min, 4 °C. Next, cell pellets were lysed in 15 ml lysis buffer (1% triton-X-100, 10 mM $MgCl_2$, 5 mM $CaCl_2$, 20 mM HEPES, 10 mM imidazole, 150 mM NaCl, 5 mM DTT, 10 µg/ml aprotinin, 10 µg/ml leupeptin, 1 µg/ml PMSF). Cell lysates were sonicated for 7.5 min (10 sec on and 10 sec off) and centrifuged at 18000 *g*, 20 min, 4 °C. Clarified lysate was incubated with 1 mL equilibrated Ni-NTA affinity agarose (Qiagen) for 60 min at 4 °C. Resin with bound protein was applied to a 1 mL column (Qiagen) and washed with 5 ml wash buffer (20 mM HEPES, 150 mM NaCl, 10 mM imidazole), 5 ml high salt wash buffer (20 mM HEPES, 500 mM NaCl, 10 mM imidazole), and again with 5 ml wash buffer. Protein was eluted with 2 ml elution buffer (20 mM HEPES, 150 mM NaCl, and varying concentrations of imidazole (70 mM-250 mM)). Eluted fractions were applied to size-exclusion chromatography (Superdex 200 increase 10/300 GL column (Cytiva), equilibrated in buffer containing 200 mM HEPES, 400 mM NaCl). Purified protein was analyzed via SDS-PAGE with Coomassie blue staining, quantified by absorbance (A280, Nanodrop one^c, ThermoFisher) and diluted in binding buffer (20 mM HEPES, 145 mM NaCl, 10 mM KCl, 5 mM $MgCl_2$, 1 mM DTT, 1% sucrose) and aliquoted for long-term storage at −80 °C.

PDZ1-GPCR C-tail binding assay

Black 96-well flat-, glass-bottom plates (Greiner Bio-One) were coated with 100 µg/ml neutravidin (Invitrogen) in 0.1 M sodium bicarbonate (pH 9.6) at 4 °C, overnight. Next day, wells were blocked with binding buffer (20 mM HEPES, 145 mM NaCl, 10 mM KCl, 5 mM $MgCl_2$) containing 0.1% BSA for 60 min at room temperature. The blocking solution was aspirated and plates were stored at 4 °C until use. Purified PDZ1 domain was biotinylated using SNAP-surface biotin Alexa Flour 647 (NEB) following manufacturer's instructions. Biotinylated PDZ1 domain (2 µM) was added to neutravidin coated well in the prepared 96-well plate (100 µl/well) and incubated for 20–25 min at room temperature. Excess protein was washed off with 100 µl binding buffer containing 1 mg/mL BSA, twice. Matched concentration of distinct GPCR C-tails (100 nM) was used to assess the strength of interaction. mCitrine-GPCR C-tail (100 nM; VIPR1, LPA1R, D2R, and V2R C-tails purified from Sf9, see Sf9 protein expression and purification) was added to wells (100 µl/well) and incubated for 90 min at room temperature. Finally, wells were washed with 100 µl binding buffer containing 1 mg/ml BSA and fluorescence for mCitrine was measured (excitation 495 nm, emission 525 nm; Tecan Spark). Control for each GPCR C-tail (no PDZ1) was subtracted from the respective sample condition and normalized to VIPR1 C-tail. 3 technical and 3 biological replicates were performed for each condition.

Statistics and reproducibility

All experiments were performed at least three times to ensure reproducibility. Number of biological replicates is listed in figure legends and methods. Specific description of data analysis for each experiment is defined in the relevant sub-sections of methods. In general, unpaired t-test was performed when comparing two conditions, while one-way ANOVA with Tukey's or Dunnett's post hoc test was performed for comparison of three or more conditions. All data graphs were generated in GraphPad Prism and statistical analysis was performed using GraphPad Prism (10.2.0). Data is presented as mean +/- standard deviation (SD) with number of technical and biological replicates indicated in figure legends and methods section. Matching symbol shape across different conditions indicates biological replicates.

Reporting summary

Further information on research design is available in the Nature Portfolio Reporting Summary linked to this article.

Data availability

All data pertaining to this study are presented in the main figures and Supplementary Figs. Additional data figures and images are available upon request from the corresponding author. Source data are provided with this paper.

References

1. Von Zastrow, M. & Sorkin, A. Mechanisms for regulating and organizing receptor signaling by endocytosis. *Annu. Rev. Biochem.* **90**, 709–737 (2021).

2. Weinberg, Z. Y. & Puthenveedu, M. A. Regulation of G protein-coupled receptor signaling by plasma membrane organization and endocytosis. *Traffic* **20**, 121–129 (2019).
3. Weis, W. I. & Kobilka, B. K. The Molecular Basis of G Protein-Coupled Receptor. *Annu. Rev. Biochem.* **87**, 897–919 (2018).
4. Dunn, H. A. & Ferguson, S. S. G. PDZ protein regulation of g protein-coupled receptor trafficking and signaling pathways. *Mol. Pharmacol.* **88**, 624–629 (2015).
5. Romero, G., Von Zastrow, M. & Friedman, P. A. *Role of PDZ Proteins in Regulating Trafficking, Signaling, and Function of GPCRs. Means, Motif, and Opportunity*. *Advances in Pharmacology* **62**, (Elsevier Inc., 2011).
6. Harris, B. Z. & Lim, W. A. Mechanism and role of PDZ domains in signaling complex assembly. *J. Cell Sci.* **114**, 3219–3231 (2001).
7. Mahon, M. J., Donowitz, M., Yun, C. C. & Segre, G. V. Na+/H+ exchanger regulatory factor 2 directs parathyroid hormone 1 receptor signalling. *Nature* **417**, 858–861 (2002).
8. Lee, H. & Zheng, J. J. PDZ domains and their binding partners: structure, specificity, and modification AR. *Cell Commun. Signal.* **8**, 1–18 (2010).
9. Ford, C. P. The role of D2-autoreceptors in regulating dopamine neuron activity and transmission. *Neuroscience* **282**, 13–22 (2014).
10. Missale, C., Russel Nash, S., Robinson, S. W., Jaber, M. & Caron, M. G. Dopamine receptors: From structure to function. *Physiol. Rev.* **78**, 189–225 (1998).
11. Bonci, A. & Hopf, F. W. The dopamine D2 receptor: New surprises from an old friend. *Neuron* **47**, 335–338 (2005).
12. Jeanneteau, F., Diaz, J., Sokoloff, P. & Griffon, N. Interactions of GIPC with dopamine D2, D3 but not D4 receptors define a novel mode of regulation of g protein-coupled receptors. *Mol. Biol. Cell* **15**, 696–705 (2004).
13. Jeanneteau, F., Guillin, O., Diaz, J., Griffon, N. & Sokoloff, P. GIPC recruits GAIP (RGS19) to attenuate dopamine d2 receptor signaling. *Mol. Biol. Cell* **15**, 4926–4937 (2004).
14. Hirakawa, T., Galet, C., Kishi, M. & Ascoli, M. GIPC binds to the human lutropin receptor (hLHR) through an unusual PDZ domain binding motif, and it regulates the sorting of the internalized human choriogonadotropin and the density of cell surface hLHR. *J. Biol. Chem.* **278**, 49348–49357 (2003).
15. Varsano, T., Taupin, V., Guo, L., Baterina, O. Y. & Farquhar, M. G. The PDZ protein GIPC regulates trafficking of the LPA1 receptor from appl signaling endosomes and attenuates the cell's response to LPA. *PLoS One* **7**, e49227 (2012).
16. Hu, L. A. et al. GIPC interacts with the β1-adrenergic receptor and regulates β1-adrenergic receptor-mediated ERK activation. *J. Biol. Chem.* **278**, 26295–26301 (2003).
17. Aschenbrenner, L., Lee, T. & Hasson, T. Myo6 facilitates the translocation of endocytic vesicles from cell peripheries. *Mol. Biol. Cell* **14**, 2728–2743 (2003).
18. Dance, A. L. et al. Regulation of myosin-VI targeting to endocytic compartments. *Traffic* **5**, 798–813 (2004).
19. Hartman, M. A., Finan, D., Sivaramakrishnan, S. & Spudich, J. A. Principles of unconventional myosin function and targeting. *Annu. Rev. Cell Dev. Biol.* **27**, 133–155 (2011).
20. Tumbarello, D. A., Kendrick-Jones, J. & Buss, F. Myosin VI and its cargo adaptors -linking endocytosis and autophagy. *J. Cell Sci.* **126**, 2561–2570 (2013).
21. Magistrati, E. & Polo, S. Myomics: myosin VI structural and functional plasticity. *Curr. Opin. Struct. Biol.* **67**, 33–40 (2021).
22. Buss, F., Spudich, G. & Kendrick-jones, J. MYOSIN VI: cellular functions and motor properties. *Cell Dev. Biol.* **20**, 649–676 (2004).
23. Rai, A. et al. Multimodal regulation of myosin VI ensemble transport by cargo adaptor protein GIPC. *J. Biol. Chem.* **298**, 101688 (2022).
24. Naccache, S., Hasson, T. & Horowitz, A. Binding of internalized receptors to the PDZ domain of GIPC/synectin recruits myosin VI to endocytic vesicles. *PNAS* **103**, 15272–15273 (2006).
25. Varsano, T. et al. GIPC is recruited by APPL to peripheral TrkA endosomes and regulates TrkA trafficking and signaling. *Mol. Cell. Biol.* **26**, 8942–8952 (2006).
26. Bunn, R. C., Jensen, M. A. & Reed, B. C. Protein interactions with the glucose transporter binding protein GLUT1CBP that provide a link between GLUT1 and the cytoskeleton. *Mol. Biol. Cell* **10**, 819–832 (1999).
27. Heissler, S. M. et al. Kinetic properties and small-molecule inhibition of human myosin-6. *FEBS Lett* **586**, 3208–3214 (2012).
28. Sundaramoorthy, V. et al. Defects in optineurin- and myosin VI-mediated cellular trafficking in amyotrophic lateral sclerosis. *Hum. Mol. Genet.* **24**, 3830–3846 (2015).
29. Hari-Gupta, Y. et al. Myosin VI regulates the spatial organisation of mammalian transcription initiation. *Nat. Commun.* **13**, 1–18 (2022).
30. Wagner, W. et al. Myosin VI drives clathrin-mediated AMPA receptor endocytosis to facilitate cerebellar long-term depression. *Cell Rep* **28**, 11–20.e9 (2019).
31. Shang, G. et al. Structure analyses reveal a regulated oligomerization mechanism of the PlexinD1/GIPC/myosin VI complex. *Elife* **6**, 1–25 (2017).
32. Lin, Y. H. et al. Accumbal D2R-medium spiny neurons regulate aversive behaviors through PKA-Rap1 pathway. *Neurochem. Int.* **143**, 104935 (2021).
33. Hasson, T. Myosin VI: Two distinct roles in endocytosis. *J. Cell Sci.* **116**, 3453–3461 (2003).
34. Osterweil, E., Wells, D. G. & Mooseker, M. S. A role for myosin VI in postsynaptic structure and glutamate receptor endocytosis. *J. Cell Biol.* **168**, 329–338 (2005).
35. Nash, J. E. et al. Disruption of the interaction between myosin VI and SAP97 is associated with a reduction in the number of AMPARs at hippocampal synapses. *J. Neurochem.* **112**, 677–690 (2010).
36. Zhuang, Y. et al. Structural insights into the human D1 and D2 dopamine receptor signaling complexes. *Cell* **184**, 931–942.e18 (2021).
37. Beom, S. R., Cheong, D., Torres, G., Caron, M. G. & Kim, K. M. Comparative studies of molecular mechanisms of dopamine D2 and D3 receptors for the activation of extracellular signal-regulated kinase. *J. Biol. Chem.* **279**, 28304–28314 (2004).
38. Sivaramakrishnan, S., Schneider, J. L., Sitikov, A., Goldman, R. D. & Ridge, K. M. Shear stress induced reorganization of the keratin intermediate filament network requires phosphorylation by protein kinase C. *Mol. Biol. Cell* **20**, 2673–2683 (2009).
39. Kim, K. M. et al. Differential regulation of the dopamine d2 and d3 receptors by g protein-coupled receptor kinases and β-arrestins. *J. Biol. Chem.* **276**, 37409–37414 (2001).
40. Vickery, R. G. & Von Zastrow, M. Distinct dynamin-dependent and -independent mechanisms target structurally homologous dopamine receptors to different endocytic membranes. *J. Cell Biol.* **144**, 31–43 (1999).
41. Kabbani, N., Jeromin, A. & Levenson, R. Dynamin-2 associates with the dopamine receptor signalplex and regulates internalization of activated D2 receptors. *Cell. Signal.* **16**, 497–503 (2004).
42. Damke, H., Baba, T., Van Der Bliek, A. M. & Schmid, S. L. Clathrin-independent pinocytosis is induced in cells overexpressing a temperature-sensitive mutant of dynamin. *J. Cell Biol.* **131**, 69–80 (1995).
43. Robertson, M. J., Deane, F. M., Robinson, P. J. & McCluskey, A. Synthesis of Dynole 34-2, Dynole 2-24 and Dyngo 4a for investigating dynamin GTPase. *Nat. Protoc.* **9**, 851–870 (2014).
44. Traub, L. M. Tickets to ride: Selecting cargo for clathrin-regulated internalization. *Nat. Rev. Mol. Cell Biol.* **10**, 583–596 (2009).

45. Kang, D. S., Tian, X. & Benovic, J. L. *β-Arrestins and G protein-coupled receptor trafficking*. *Methods in Enzymol.* **521**, (Elsevier Inc., 2013).
46. Latorraca, N. R. et al. How GPCR Phosphorylation Patterns Orchestrate Arrestin-Mediated Signaling. *Cell* **183**, 1813–1825.e18 (2020).
47. Yang, Z. et al. Phosphorylation of g protein-coupled receptors: From the barcode hypothesis to the flute model. *Mol. Pharmacol.* **92**, 201–210 (2017).
48. Chen, H., Zhang, S., Zhang, X. & Liu, H. QR code model: a new possibility for GPCR phosphorylation recognition. *Cell Commun. Signal.* **20**, 1–16 (2022).
49. Peterson, S. M. et al. Elucidation of G-protein and β-arrestin functional selectivity at the dopamine D2 receptor. *Proc. Natl. Acad. Sci. USA* **112**, 7097–7102 (2015).
50. Oakley, R. H., Laporte, A., Holt, J. A., Barak, L. S. & Caron, M. G. Association of B-Arrestin with G Protein-coupled Receptors during Clathrin-mediated Endocytosis Dictates the Profile of Receptor Resensitization. *J. Biol. Chem.* **274**, 32248–32257 (1999).
51. Daly, C. et al. B-arrestin-dependent and -independent endosomal G protein activation by the vasopressin type 2 receptor. *Elife* 1–19. (2023).
52. Jean-Alphonse, F. et al. Spatially restricted G protein-coupled receptor activity via divergent endocytic compartments. *J. Biol. Chem.* **289**, 3960–3977 (2014).
53. Hanyaloglu, A. C., McCullagh, E. & Von Zastrow, M. Essential role of Hrs in a recycling mechanism mediating functional resensitization of cell signaling. *EMBO J* **24**, 2265–2283 (2005).
54. Spudich, J. A. & Sivaramakrishnan, S. Myosin VI: An innovative motor that challenged the swinging lever arm hypothesis. *Nat. Rev. Mol. Cell Biol.* **11**, 128–137 (2010).
55. Henkel, B., Bintig, W., Bhat, S. S., Spehr, M. & Neuhaus, E. M. NHERF1 in microvilli of vomeronasal sensory neurons. *Chem. Senses* **42**, 25–35 (2016).
56. Saro, D. et al. A thermodynamic ligand binding study of the third PDZ domain (PDZ3) from the mammalian neuronal protein PSD-95. *Biochemistry* **46**, 6340–6352 (2007).
57. Ritt, M. & Sivaramakrishnan, S. Engaging myosin VI tunes motility, morphology and identity in endocytosis. *Traffic* **19**, 710–722 (2018).
58. Patel, N. M. et al. KIF13A motors are regulated by Rab22A to function as weak dimers inside the cell. *Sci. Adv.* **7**, eabd2054 (2021).
59. Tuplin, E. W. & Holahan, M. R. Aripiprazole, a drug that displays partial agonism and functional selectivity. *Curr. Neuropharmacol.* **15**, 1192–1207 (2017).
60. Heng, J. et al. Function and dynamics of the intrinsically disordered carboxyl terminus of β2 adrenergic receptor. *Nat. Commun.* **14**, 2005 (2023).
61. Sadler, F. et al. Autoregulation of GPCR signalling through the third intracellular loop. *Nature* **615**, 734–741 (2023).
62. Sivaramakrishnan, S. & Spudich, J. A. Systematic control of protein interaction using a modular ER/K -helix linker. *Proc. Natl. Acad. Sci.* **108**, 20467–20472 (2011).
63. Xiao, M. F. et al. Neural cell adhesion molecule modulates dopaminergic signaling and behavior by regulating dopamine D2 receptor internalization. *J. Neurosci.* **29**, 14752–14763 (2009).
64. Yi, Z. et al. The role of the PDZ protein GIPC in regulating NMDA receptor trafficking. *J. Neurosci.* **27**, 11663–11675 (2007).
65. Wieman, H. L. et al. An essential role for the Glut1 PDZ-Binding Motif in Growth Factor Regulation of Glut1 Degradation and Traffikcing. *Biochem J* **418**, 345–367 (2009).
66. Lou, X., Yano, H., Lee, F., Chao, M. V. & Farquhar, M. G. GIPC and GAIP form a complex with TrkA: A putative link between G protein and receptor tyrosine kinase pathways. *Mol. Biol. Cell* **12**, 615–627 (2001).
67. Avraham, K. B. et al. The mouse Snell's waltzer deafness gene encodes an unconventional myosin required for structural integrity of inner ear hair cells. *Nature* **11**, 369–375 (1995).
68. Avraham, K. B. et al. Characterization of unconventional MYO6, the human homologue of the gene responsible for deafness in Snell's waltzer mice. *Hum. Mol. Genet.* **6**, 1225–1231 (1997).
69. Melchionda, S. et al. MYO6, the human homologue of the gene responsible for deafness in Snell's waltzer mice, is mutated in autosomal dominant nonsyndromic hearing loss. *Am. J. Hum. Genet.* **69**, 635–640 (2001).
70. Mohiddin, S. A. et al. Novel association of hypertrophic cardiomyopathy, sensorineural deafness, and a mutation in unconventional myosin VI (MYO6). *J. Med. Genet.* **41**, 309–314 (2004).
71. Gotoh, N. et al. Altered renal proximal tubular endocytosis and histology in mice lacking myosin-VI. *Cytoskeleton* **67**, 178–192 (2010).
72. O'Loughlin, T., Masters, T. A. & Buss, F. The MYO6 interactome reveals adaptor complexes coordinating early endosome and cytoskeletal dynamics. *EMBO Rep.* **19**, 1–16 (2018).
73. Shapiro, D. A. et al. Aripiprazole, a novel atypical antipsychotic drug with a unique and robust pharmacology. *Neuropsychopharmacology* **28**, 1400–1411 (2003).
74. Mallet, J., Gorwood, P., Le Strat, Y. & Dubertret, C. Major Depressive Disorder (MDD) and Schizophrenia- Addressing Unmet Needs with Partial Agonists at the D2 Receptor: A Review. *Int. J. Neuropsychopharmacol.* **22**, 651–664 (2019).
75. Grundmann, M. et al. Lack of beta-arrestin signaling in the absence of active G proteins. *Nat. Commun.* **9**, 1–7 (2018).
76. Blythe, E. E. & von Zastrow, M. β-Arrestin-independent endosomal cAMP signaling by a polypeptide hormone GPCR. *Nat. Chem. Biol.* https://doi.org/10.1038/s41589-023-01412-4 (2023).
77. Wan, Q. et al. Mini G protein probes for active G protein– coupled receptors (GPCRs) in live cells. *J. Biol. Chem.* **293**, 7466–7473 (2018).
78. Hegron, A. et al. Therapeutic antagonism of the neurokinin 1 receptor in endosomes provides sustained pain relief. *PNAS* **120**, e2220979120 (2023).
79. Gnanapragasam, M. N. et al. p66α - MBD2 coiled-coil interaction and recruitment of Mi-2 are critical for globin gene silencing by the MBD2 - NuRD complex. *Proc. Natl. Acad. Sci. USA* **108**, 7487–7492 (2011).
80. Schindelin, J. et al. Fiji: An open-source platform for biological-image analysis. *Nat. Methods* **9**, 676–682 (2012).
81. Sommese, R. F., Sivaramakrishnan, S., Baldwin, R. L. & Spudich, J. A. Helicity of short E-R/K peptides. *Protein Sci.* **19**, 2001–2005 (2010).

Acknowledgements

We thank Michael Ritt, Fredrik Sadler, and Duha Vang for their feedback on the manuscript. This research was funded by the NIH (R35-GM126940 to S.S., R01-DA012864 to M.v.Z., R01NS1027722 to N.W.B., R01DE029951 to N.W.B., R01DK118971 to N.W.B., RM1 DE033491 to N.W.B., and 5K12GM119955-07 to N.M.P.) and Department of Defense (W81XWH-22-1-0238 to N.W.B.). L.R. was supported by the European Molecular Biology Organization (ALTF 192-2019).

Author contributions

N.M.P. and S.S. designed the study. L.R. performed experiments in MSNs. C.J.P. performed ebBRET experiments. E.E.B. generated HEK293 Δβ-arr cells. N.M.P. performed all other experiments and analyzed data. N.M.P., N.M., N.V., N.W.B, M.v.Z., and S.S. assisted with data analysis and writing of the manuscript.

Competing interests

S.S. is co-founder of Oxbow Therapeutics, LLC. N.W.B is a founding scientist of Endosome Therapeutics. The remaining authors declare no competing interests.

Additional information

Supplementary information The online version contains supplementary material available at https://doi.org/10.1038/s41467-024-55053-9.

Correspondence and requests for materials should be addressed to Sivaraj Sivaramakrishnan.

Peer review information *Nature Communications* thanks Serdar Durdagi, and the other, anonymous, reviewer(s) for their contribution to the peer review of this work. A peer review file is available.